JGR Solid Earth

RESEARCH ARTICLE
10.1029/2019JB018873

Dynamics of the Gibraltar Arc System: A Complex Interaction Between Plate Convergence, Slab Pull, and Mantle Flow

Chiara Civiero[1,2], Susana Custódio[2], João C. Duarte[2,3,4], Virgilio B. Mendes[2], and Claudio Faccenna[5]

[1]Geophysics Section, Dublin Institute for Advanced Studies (DIAS), Dublin, Ireland, [2]Instituto Dom Luiz (IDL), Faculdade de Ciências, Universidade de Lisboa, Lisbon, Portugal, [3]Departamento de Geologia, Faculdade de Ciências, Universidade de Lisboa, Lisbon, Portugal, [4]School of Earth, Atmosphere and Environment, Monash University, Melbourne, Victoria, Australia, [5]Dipartimento di Scienze Geologiche, Università di Roma Tre, Rome, Italy

Key Points:
- The Gibraltar subduction is undergoing a phase of progressive lateral disruption, with some segments still attached to the surface in the Rif and western Betics
- The slab appears segmented into two domains, one north and the other south of the Gibraltar strait; the segmentation is likely driven by Eurasia-Nubia convergence
- Mantle flow around the slab seems still active and causing most of the surface uplift, although the slab is not retreating anymore

Supporting Information:
- Supporting Information S1

Correspondence to:
C. Civiero,
cciviero@cp.dias.ie

Citation:
Civiero, C., Custódio, S., Duarte, J. C., Mendes, V. B., & Faccenna, C. (2020). Dynamics of the Gibraltar arc system: A complex interaction between plate convergence, slab pull, and mantle flow. *Journal of Geophysical Research: Solid Earth*, *125*, e2019JB018873. https://doi.org/10.1029/2019JB018873

Received 11 OCT 2019
Accepted 17 APR 2020
Accepted article online 23 APR 2020

Abstract In typical subduction systems, plate convergence is subperpendicular to the trench. The Gibraltar Arc System is exceptional, with its narrow subduction arc oriented N-S and laterally "squeezed" by the NNW-SSE tectonic convergence between Nubia and Iberia. The extent to which the slab is still coupled to the surface and how it interacts actively with the surrounding mantle is a matter of ongoing debate. Here, we analyze new densely spaced GPS data, together with crustal and mantle observations, to better understand the slab kinematics, plate dynamics, and mantle flow. In light of previous and current research, we find that subduction below the Gibraltar Arc is currently in the middle of a disruption process, with parts of it already detached and others yet coupled to the surface. In particular, the slab seems to be detached to the north of the Gibraltar Strait, with a small portion still attached to the surface or in the process of detaching below the western Betics. South of Gibraltar, the slab is still coupled to the overriding plate, although the subduction seems to be very slow or stopped. Flow of mantle material around the detached portions of the slab causes most of the surface uplift and a positive residual topography anomaly. Our findings show that the interplay between slab dynamics, mantle flow, and plate convergence explains much of the observed residual topography, surface motion, seismicity, and mantle structure.

1. Introduction

The Gibraltar Arc System is located within the plate boundary zone that separates Nubia (NW Africa) from Iberia (SW Europe), marking the western termination of the Mediterranean orogenic belt (Faccenna et al., 2014; Royden, 1993) (Figure 1). It comprises a tightly arcuate mountain chain, the Rif-Betics chain, and the extensional arc-back-arc domain of the Alboran basin. Both these domains have formed since ~30 Ma, under the influence of the oblique dextral plate convergence of the Nubian and Eurasian plates (Faccenna et al., 2004; Malinverno & Ryan, 1986; Rehault et al., 1985; Rosenbaum et al., 2002). The origin of this complex system, in particular its association with a possible subduction zone, is a matter of controversy. Contrasting models have been proposed to explain the extension of the Alboran region and the contemporaneous formation of the Betic-Rif orogen, including lithospheric delamination (e.g., Calvert et al., 2000; Platt & Vissers, 1989; Seber et al., 1996; Williams & Platt, 2018) and subduction and rollback models (Casciello et al., 2015; Chertova et al., 2014; Chevrot et al., 2014; Faccenna et al., 2004; Gutscher et al., 2002; Lonergan & White, 1997; Platt et al., 2013; Royden, 1993; Van Hinsbergen et al., 2014; Vergés & Fernàndez, 2012; Wortel & Spakman, 2000). However, an agreement on the origin and current dynamics of the system is yet to be reached.

The Gibraltar Arc System is currently trapped between the NNW-SSE converging Nubia and Eurasian plates, which move with respect to each other at a rate of 4.5–6 mm yr^{-1} in the region (Fernandes et al., 2003). Detailed geodetic data (Fadil et al., 2006; Koulali et al., 2011; Palano et al., 2013; Pérouse et al., 2010) and numerical modeling (e.g., Jiménez-Munt & Negredo, 2003; Neres et al., 2016; Spakman et al., 2018) corroborate that plate subduction may provide a plausible mechanism for driving surface deformation. However, in spite of previous efforts, the drivers of present-day surface deformation remain poorly constrained. Topographic variations and geodetic displacements may be related to processes acting at different levels,

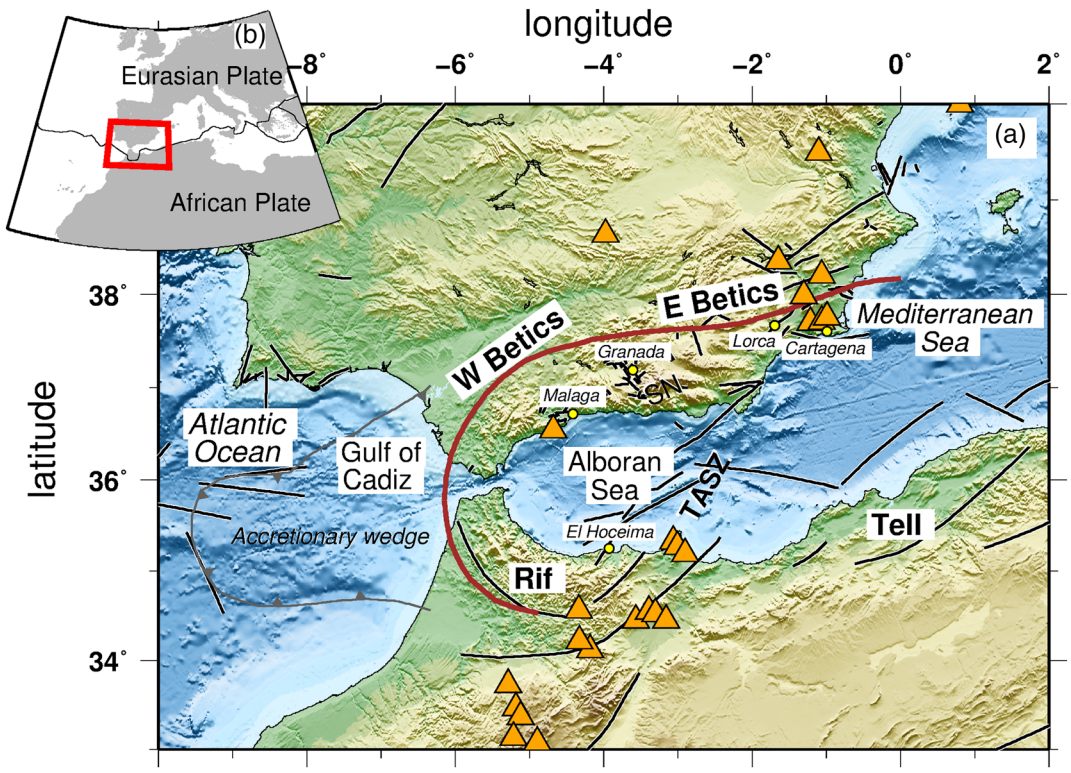

Figure 1. (a) Topography of the Gibraltar arc region from SRTM30+ (Smith & Sandwell, 1997). The main fault traces identified on the SHARE database (Basili et al., 2013; Vilanova et al., 2014) are shown in black; the Gibraltar arc (from Neres et al., 2016) and the accretionary wedge fault (after Gutscher et al., 2002) are indicated in brown and gray, respectively. The same fault and arc traces are plotted in all the figures. Cenozoic volcanic fields are represented with orange triangles (modified from Lustrino & Wilson, 2007). The geographic features cited in the text are indicated in black. SN: Sierra Nevada; TASZ: Trans-Alboran shear zone. (b) Location of the study area along the Eurasia-Africa plate boundary (red rectangle). The black line shows the plate boundaries from Bird (2003).

from the crust to the deep mantle: (1) Shallow processes, such as tectonic deformation due to plates' relative motion, surface erosion, and sediment deposition, lead to temporal changes in crustal or lithospheric thickness. The resulting isostatic adjustment may lead to changes in elevation, translated in surface uplift or subsidence in the geodetic signal (Molnar & England, 1990); (2) deep processes may also cause both horizontal and vertical surface deformation, mostly through mantle flow inducing stresses at the base of the lithosphere (Faccenna et al., 2014; Hager et al., 1984). While independent studies are generally not capable of quantifying how much of the surface motion is due to lithospheric versus sublithospheric processes, the integration of data across several fields of the Earth sciences can help to better identify which processes are active and where they prevail.

In the present work, we first reconstruct the velocity and the strain rates of the Gibraltar Arc System region using Global Positioning System (GPS) data from continuous stations and episodic campaigns, spanning the period 1995–2019. The dense GPS network allows us to obtain, for the first time, a high-resolution image of horizontal and vertical surface deformation of the study area. We then comparatively analyze this new dataset with up-to-date seismicity, crustal, and mantle observations to gain new insights into the complex structure of the Gibraltar Arc System and on how surface deformation is related to the interactions between lithospheric and sublithospheric processes.

2. GPS Data and Method

Over the past 20 years, the increasing number of GPS stations in the Gibraltar Arc System allowed for the computation of denser and more precise surface velocity fields (Fadil et al., 2006; Garate et al., 2015; Koulali et al., 2011; Mancilla et al., 2013; Serpelloni et al., 2013; Stich et al., 2006; Tahayt et al., 2008;

Vernant et al., 2010). These have served to constrain plate kinematics, geodynamics, and active tectonics along the Nubia-Eurasia plate boundary. However, in most cases, only horizontal velocities were investigated, while the analysis of vertical velocities remained a challenge. Worldwide, the use of vertical GPS rates has been mostly limited to sea level measurements (e.g., Becker et al., 2002; Teferle et al., 2006; Wöppelmann et al., 2007), postglacial rebound (e.g., Larson & van Dam, 2000; Scherneck et al., 2001), volcanic monitoring (Lowry et al., 2001), and anthropogenic or natural subsidence (e.g., Abidin et al., 2008). On a regional scale, Serpelloni et al. (2013) provided a first map of vertical velocities over the entire Euro-Mediterranean domain, but the distribution of GPS stations was nonuniform and quite sparse in some areas, namely, in the Iberia domain.

Here, we present a new GPS dataset that provides a detailed synoptic view of surface velocities in the region (Figure 2). We processed GPS observations from ~140 continuous stations in Iberia, covering a period of over 25 years (1995.6–2019.5). The data set is available through the International GNSS Service (Johnston et al., 2017) and EUREF (Bruyninx et al., 2012) and includes also data from regional networks. Additional data from campaign sites enriched the data set, namely, from stations in Morocco, spanning the 1999–2006 time interval (available at the UNAVCO archive, http://www.unavco.org). The GPS data were processed using the GAMIT/GLOBK software package (Herring et al., 2015). First, we used a double-differenced, ionosphere-free linear combination of L1 and L2 carrier phases to estimate loosely constrained station coordinates, satellite state vectors, and other parameters, along with the associated variance-covariance matrices. At this stage, we used precise orbits from ESA/ESOC, absolute antenna phase center models from IGS, ocean tide loading corrections from the FES2004 ocean tide model (Lyard et al., 2006), and Earth tide corrections according to the IERS Conventions (2010). In order to model the neutral atmospheric refraction, we used a priori zenith delays from GPT2 model (Lagler et al., 2013), mapped with the VMF mapping functions (Boehm et al., 2006), complemented with station zenith delays corrections estimated at each station at 1-hr intervals, and station gradients parameters in north-south and east-west directions at 24-hr intervals. Our solutions are expressed in the ITRF2008 reference frame (Altamimi et al., 2011). Second, GAMIT solutions were used to obtain a consistent set of daily station position time series for all sites, which were visually screened for outliers and discontinuities. To account for time-correlated noise, we applied the realistic sigma method (Herring, 2003).

Current surface vertical motions in Europe are strongly affected by ongoing postglacial rebound processes (Johansson, 2002; Nocquet et al., 2005). Therefore, we estimated the vertical motion due to glacial isostatic adjustment (GIA) at GPS sites considering the ICE6G(VM5a) model (Peltier et al., 2015). This model shows a pattern of subsidence in the Gibraltar Arc System while surface uplift is predicted in Central Iberia (Figure S1 in the supporting information). Notably, the correction of GPS velocities for the GIA contribution results in slightly increased rates of uplift in the Betics and Rif (Figure S2).

We then use the spherical wavelet-based multiscale method proposed by Tape et al. (2009) to compute spatial velocity fields from our irregularly spaced GPS observations. In particular, we present the strain rate and the dilatation rate fields. The strain rate field is computed as the Frobenius norm of the strain rate tensor and therefore quantifies the summed squared contributions from all strain tensor components. The dilatation rate field, or volumetric strain rate, is the divergence of the velocity field, or, equivalently, the first invariant of the velocity gradient tensor, thus quantifying the amount of dilatation/compression that affects a given region.

3. GPS Results

Figures 2a and 2b Illustrate the horizontal velocities relative to the Nubia and Eurasia plates, respectively, considering the ITRF2008-PMM model (Altamimi et al., 2012). In Table 1 we show the displayed velocities expressed in mm/yr. Sites located within the northern Rif domain in Morocco show overall SW motions (~1–2 mm/yr, with most of the velocities lower than error bars) with respect to Nubia, while in the southern Rif the movement is predominantly S-SE directed (Figure 2a). The 2-D strain rate field shows moderate strain rate values in the Rif, reaching ~7×10^{-9} yr^{-1} (Figure 2a). The dilatation rate is negative, ~-2×10^{-9} yr^{-1}, implying that the region is undergoing shortening (Figure 2b). In a fixed Eurasia reference frame (Figure 2b), sites located in the Betics, north of the Alboran Sea, have a well-defined W-SW–oriented motion, albeit at low rates of ~0.5–1.5 mm/yr. Strain rates in this region are

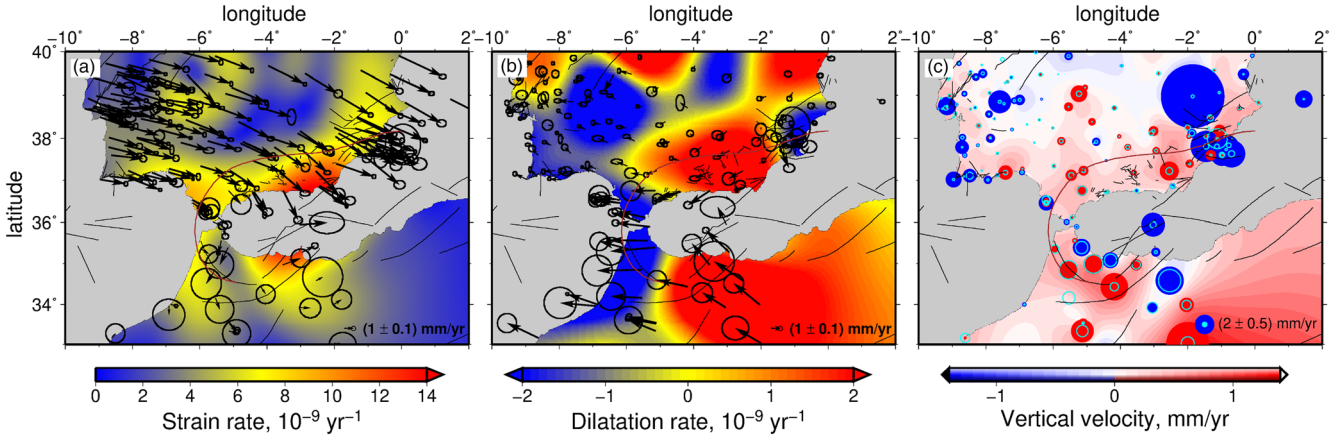

Figure 2. Horizontal velocity estimates from GPS (black vectors tipped with 95% confidence error ellipse). (a) GPS velocities in a Nubian-fixed reference frame. The colored background shows the strain rate field. (b) GPS velocities in a Eurasian-fixed reference frame. The colored background shows the dilatation rate field. (c) Vertical velocity estimates from GPS data are represented with circles (before GIA correction). The associated error is represented with light blue circles. Positive (red) is upward, and negative (blue) is downward motion. The colored background is the vertical velocity field as smoothed from the geodetic data (after GIA correction) and used in profiles of Figure 8. Note that campaign sites have uncertainties much larger than continuous sites.

slightly higher than those observed in the Rif, reaching values of 8×10^{-9} yr^{-1} in western Betics and ~12×10^{-9} yr^{-1} in eastern Betics. Although the region directly north of the Gibraltar Strait is undergoing shortening, most of the Betics are characterized by a positive dilatation rate field, on the order of 2×10^{-9} yr^{-1}, indicating that extension currently dominates the region. Figure 2c shows vertical velocities, highlighting areas of consistent uplift and subsidence. Low rates of uplift are consistently observed in the Betics (~0.5–2.0 mm/yr). Moving southward, in the Rif, the uplift rate is faster, between ~2 and 3 mm/yr in turn, the most significant subsidence rates are ~3 mm/yr and observed east of the trans-Alboran shear zone (TASZ), in southeast Iberia around Cartagena and east of El Hoceima, although the latter is poorly constrained. Around Lorca, in East Iberia, we observe an extremely high value of subsidence (>5 mm/yr), which likely results from the intensive agriculture and overexploitation of aquifers that take place in SE Spain (Fernandez et al., 2018; Pulido-Bosch et al., 2012); therefore, we will not take it into account in our interpretation. The highest computed strain rate values are observed along the TASZ, both north and south of the Alboran Sea, reaching values of ~14×10^{-9} yr^{-1} (Figure 2a).

4. Crustal and Mantle Observations

4.1. Seismicity

Earthquakes along the Gibraltar Arc display a complex pattern that mimics the complexity of the tectonic framework (Figure 3). Lithospheric deformation generates a 400-km wide EW-running seismicity belt (Buforn et al., 1995). North of the Gibraltar Strait (~36° N), earthquakes spread throughout the Betics, sometimes clustering locally. Here, the focal mechanisms are diverse, pointing to multiple driving forces at work (Custódio et al., 2016; Martín et al., 2015; Stich et al., 2005, 2020). In the westernmost Betics, focal mechanisms indicate thrust and strike-slip faulting, in agreement with plate convergence. Moving eastward along southern Spain, the Granada basin hosts earthquakes with predominantly normal focal mechanisms. Five very deep (600–650 km, M4.3–7.8) earthquakes have been recorded below Granada since the mid-twentieth century (Buforn et al., 1991, 2011; Mancilla et al., 2012), with focal mechanisms indicating faulting along either subvertical or subhorizontal planes. These events have been tentatively associated with a remnant lithospheric body, located between 630 and 660 km depth, fracturing beneath southern Iberia (Blanco & Spakman, 1993; Piromallo & Morelli, 2003) or with shear melting along a horizontal plane inside the subducted slab near the 660-km discontinuity (Buforn et al., 2011). Directly east of Granada, the Sierra Nevada, which reaches 3478 m high, is remarkably seismically silent. Further east, the SW-NE trending TASZ extends from Valencia, Spain, in the northeast, to El Hoceima, Morocco, in the southwest, crossing the Alboran Sea (Bousquet, 1978; De Larouzière et al., 1988; Leblanc & Olivier, 1984; Sanz de Galdeano, 1990). This major shear zone is overall marked by strike-slip focal mechanisms in its NE

Table 1
List of Sites and Velocities Used in This Study, Referred to the ITRF2008 Reference Frame

Station	Long (°)	Lat (°)	E	σ_E	N	σ_N	U	σ_U
BORR	−0.08321	39.90518	20.06	0.16	16.2	0.10	−0.30	0.19
VALE	−0.33765	39.48083	19.86	0.12	16.38	0.10	−1.11	0.19
ALC1	−0.47355	38.69799	19.47	0.15	16.81	0.13	0.46	0.3
ALAC	−0.48123	38.33892	19.98	0.1	16.58	0.09	0.15	0.19
TOR1	−0.68089	37.97532	19.67	0.06	17.06	0.09	−0.13	0.07
CABO	−0.6984	37.63086	20.29	0.34	17.33	0.27	−2.85	0.66
SALI	−0.77853	37.8349	19.57	0.32	16.88	0.26	−1.91	0.51
ALCA	−0.8608	37.73077	19.88	0.12	17.4	0.12	−0.35	0.27
CARG	−0.97385	37.5966	19.2	0.33	18.18	0.24	0.19	0.46
CRTG	−0.97929	37.60663	19.95	0.31	18.75	0.27	−2.25	0.6
ABAN	−1.05368	38.17506	19.48	0.11	17.34	0.11	1.22	0.08
AYOR	−1.05921	39.06134	19.07	0.11	15.89	0.11	0.15	0.22
MURC	−1.12252	37.99016	19.64	0.13	16.94	0.08	0.50	0.24
MUR2	−1.12468	37.99216	19.88	0.79	17.78	0.91	−1.31	2.16
AIRM	−1.12861	37.80652	19.17	0.26	16.28	0.21	−1.11	0.5
UTIE	−1.20859	39.56868	19.33	0.16	16.17	0.13	0.25	0.3
MAZA	−1.31049	37.59344	19.6	0.13	18.21	0.12	0.99	0.29
JUMI	−1.32565	38.50207	19.48	0.12	16.48	0.11	0.44	0.27
JUM3	−1.32716	38.47122	19.83	0.32	16.12	0.31	−0.91	0.66
CIEZ	−1.38087	38.23316	19.38	0.1	17.18	0.14	−0.04	0.28
ALHA	−1.44673	37.80424	20.69	0.25	14.19	0.19	−3.28	0.58
MULA	−1.44884	38.04111	19.19	0.23	16.46	0.21	0.35	0.49
LOR2	−1.68677	37.65389	25.1	0.38	13.03	0.34	−66.87	0.66
LORC	−1.69957	37.65791	26.76	0.22	10.94	0.20	−25.35	0.5
ALBA	−1.8564	38.97792	18.59	0.11	16.32	0.10	−6.89	0.32
CRVC	−1.86864	38.11458	20.03	0.32	15.77	0.48	−0.82	0.59
HUOV	−1.94212	37.40156	19.72	0.09	16.95	0.09	0.79	0.29
CARA	−1.96768	38.04588	18.85	0.21	15.96	0.20	0.44	0.14
MORA	−1.99882	38.24753	19.42	0.25	16.39	0.28	0.43	0.59
TNDR	−2.00301	33.03131	17.7	0.6	18.25	0.53	4.57	1.42
BMTR	−2.03269	33.9864	17.44	0.45	18.95	0.43	1.42	1.01
ALMR	−2.44088	36.86267	19.01	0.23	16.76	0.19	−0.47	0.5
ALME	−2.45945	36.85253	18.66	0.06	16.26	0.08	0.09	0.2
AION	−2.53255	34.58794	16.95	0.9	18.71	0.89	−2.93	2.45
CAAL	−2.54761	37.22109	18.02	0.28	15.76	0.28	1.98	0.75
MOTA	−2.87001	39.50321	18.43	0.19	16.08	0.18	0.08	0.43
PALC	−2.9324	37.70234	17.98	0.15	15.9	0.09	0.69	0.33
MELI	−2.95165	35.28119	17.36	0.15	19.01	0.13	−0.82	0.37
VIAR	−3.01248	38.16764	18.5	0.16	15.91	0.14	0.89	0.36
ALBO	−3.03424	35.93984	18.8	0.78	18.53	0.48	−2.46	0.71
DEBD	−3.05536	33.91874	17.6	0.47	18.25	0.44	−1.08	1.15
VICA	−3.08286	38.11764	18.48	0.25	16.4	0.20	−0.27	0.48
MOTR	−3.52052	36.75476	17.1	0.19	15.04	0.16	−0.38	0.44
MDAR	−3.53217	34.97012	17.94	0.43	18.99	0.41	1.08	0.94
GRA1	−3.5964	37.1899	18	0.23	15.97	0.12	0.49	0.13
UJAE	−3.78173	37.78776	18.52	0.19	16.01	0.19	0.61	0.41
SONS	−3.96397	39.67535	18.54	0.08	16.24	0.08	−0.29	0.23
ANDU	−4.03031	38.04038	18.84	0.15	16.98	0.14	0.32	0.1
ALMO	−4.18025	38.70551	18.11	0.19	17.23	0.36	0.31	0.53
MSLA	−4.1844	34.43172	16.52	0.43	17.4	0.42	2.90	0.93
MALA	−4.39353	36.72611	16.83	0.22	16	0.18	0.38	0.31
CABR	−4.42424	37.46796	18.29	0.09	16.92	0.09	−0.14	0.1
MLGA	−4.43541	36.7156	16.64	0.09	15.7	0.14	0.07	0.38
COBA	−4.72111	37.91561	18.25	0.1	16.67	0.12	−0.80	0.32
CRDB	−4.78783	37.8774	18.31	0.15	16.55	0.09	0.04	0.09
POZO	−4.84933	38.38347	18.27	0.16	16.31	0.1	0.66	0.11
HERR	−5.05003	39.18144	18.27	0.07	16.47	0.11	0.55	0.08
OSUN	−5.09517	37.23231	17.93	0.11	16.2	0.11	0.97	0.44
IFRN	−5.10847	33.53962	16.9	0.13	17.33	0.13	0.88	0.24
IFR1	−5.12553	33.51393	16.86	0.12	17.23	0.11	0.23	0.21

Table 1
Continued

Station	Long (°)	Lat (°)	E	σ_E	N	σ_N	U	σ_U
HEBR	−5.13117	33.33268	16.97	0.63	17.88	0.62	2.40	1.27
ROND	−5.14348	36.75404	16.52	0.45	16.64	0.44	1.01	0.98
LAOU	−5.15527	35.39494	14.61	0.63	16.24	0.62	−1.76	1.33
TALR	−5.23539	39.03508	18.63	0.23	16.93	0.22	1.67	0.59
CEU1	−5.30639	35.89197	15.61	0.15	17.1	0.13	−0.45	0.36
TETN	−5.36301	35.56164	15.14	0.08	16.71	0.06	0.46	0.16
ALGC	−5.44418	36.11104	16.19	0.21	17.35	0.16	0.34	0.46
MOFR	−5.46239	37.12072	17.55	0.27	16.92	0.24	1.06	0.57
ZAGO	−5.53127	34.15795	16.29	0.64	16.85	0.62	0.02	1.35
CATU	−5.53879	38.73043	18.22	0.07	16.73	0.07	0.82	0.08
OUZ1	−5.53916	34.85042	14.65	0.68	16.58	0.69	1.87	2.07
NAVA	−5.54512	39.89485	18.18	0.07	16.56	0.11	−0.79	0.3
TARI	−5.60262	36.00851	16.37	0.21	17.69	0.17	−0.51	0.23
CAZA	−5.75978	37.93788	17.96	0.16	17.15	0.09	0.76	0.41
TRUJ	−5.8556	39.47982	17.1	0.07	17.06	0.11	0.00	0.08
TNIN	−5.95839	35.35076	16.25	0.42	17.54	0.41	0.57	0.89
SEVI	−5.97156	37.34571	17.77	0.25	17.16	0.11	0.12	0.44
LLER	−6.01071	38.23678	17.98	0.13	16.8	0.07	0.1	0.29
SFER	−6.20565	36.46434	16.22	0.14	17.15	0.12	0.74	0.31
ROAP	−6.20627	36.46427	16.42	0.15	16.97	0.15	0.2	0.37
UCAD	−6.2105	36.53167	16.86	0.46	17.17	0.45	0.36	0.95
UCA1	−6.21186	36.53172	17.09	0.32	16.78	0.32	−0.97	0.88
MEDA	−6.34856	38.91628	17.95	0.13	17.06	0.07	−0.14	0.08
CCEX	−6.37792	39.4723	17.22	0.17	14.79	0.07	0.36	0.4
ZFRA	−6.41004	38.42601	18.2	0.13	16.53	0.11	0.15	0.29
CORI	−6.51964	39.98162	18.14	0.09	16.94	0.12	−0.14	0.35
ARAC	−6.56541	37.89388	17.63	0.25	17.16	0.13	0.05	0.15
JERE	−6.77943	38.32004	17.77	0.08	16.89	0.11	−0.12	0.19
RABT	−6.85429	33.9981	16.2	0.07	17.83	0.07	−0.34	0.17
HULV	−6.91354	37.28029	17.88	0.09	17.1	0.16	0.32	0.09
RRMT	−6.9196	33.9582	15.64	0.72	17.03	0.7	16.35	1.96
HUEL	−6.9203	37.19998	17.34	0.05	17.23	0.06	−0.52	0.24
BADJ	−6.98926	38.89369	17.81	0.14	17.44	0.15	−1.05	0.32
ELVA	−7.15941	38.87937	18.4	0.1	16.8	0.12	−0.56	0.27
AMAR	−7.22788	38.2087	17.84	0.07	17.01	0.07	−0.29	0.19
VALC	−7.24828	39.40761	17.66	0.14	16.61	0.13	−0.13	0.31
SMAM	−7.35956	39.31324	18.08	0.09	16.96	0.08	0.23	0.22
VRSA	−7.41387	37.1918	17.35	0.25	16.82	0.20	1.46	0.55
PORT	−7.43289	39.29094	17.89	0.07	16.83	0.07	−0.11	0.2
BORB	−7.46252	38.81032	18.98	0.16	16.61	0.10	−0.21	0.25
CBRA	−7.51218	39.81899	17.83	0.14	16.85	0.13	−0.03	0.46
ESTR	−7.5854	38.8466	16.6	0.17	16.83	0.09	−2.37	0.34
TVRA	−7.64091	37.1323	17.7	0.16	17.15	0.13	−0.30	0.32
MERT	−7.66005	37.64654	17.92	0.14	17.36	0.14	0.05	0.29
SMAN	−7.75199	38.45922	18.39	0.15	16.97	0.12	−0.11	0.24
BEJE	−7.8654	37.99824	18.08	0.09	16.63	0.21	−0.83	0.21
BEJ0	−7.87285	38.01288	17.71	0.07	17.22	0.07	0.27	0.18
AVIS	−7.88949	39.05661	17.63	0.15	16.79	0.14	0.22	0.3
EVOR	−7.90436	38.5681	17.86	0.07	17.05	0.08	−0.71	0.19
FARO	−7.93751	37.0164	17.35	0.07	16.8	0.07	−0.78	0.27
MOUR	−8.09446	39.50215	17.96	0.16	16.64	0.17	−0.84	0.34
BENA	−8.12669	37.23237	17.32	0.08	16.61	0.11	−0.06	0.14
MELR	−8.13042	39.69484	17.77	0.07	16.88	0.07	−0.05	0.15
QESC	−8.19938	37.13171	18.22	0.58	19.48	0.59	0.82	1.48
TRRA	−8.21918	38.29084	17.84	0.24	16.78	0.23	0.42	0.42
MESS	−8.24469	37.83463	17.71	0.1	17.03	0.07	−0.27	0.14
SMGR	−8.29366	39.42278	17.57	0.08	16.11	0.09	−0.66	0.15
FVFI	−8.32051	38.7205	17.78	0.17	17.84	0.24	−0.25	0.34
PAIA	−8.45152	39.53724	17.84	0.18	16.72	0.18	−0.29	0.34
VNOV	−8.45702	38.67862	17.76	0.09	16.98	0.08	0.09	0.22

Table 1
Continued

Station	Long (°)	Lat (°)	E	σ_E	N	σ_N	U	σ_U
ENTR	−8.47391	39.47119	17.74	0.25	17.05	0.24	0.30	0.34
VT10	−8.53464	39.23913	17.45	0.28	16.94	0.29	−2.33	0.95
SALM	−8.61946	33.1624	15.99	0.43	18.34	0.43	0.18	1.03
ODEM	−8.63125	37.59866	17.75	0.15	17.44	0.14	−0.46	0.24
GRIB	−8.64173	39.04045	17.64	0.09	17.05	0.09	−0.52	0.13
LAGO	−8.66838	37.09894	17.79	0.05	17.47	0.12	0.11	0.19
SCAC	−8.6926	38.01878	17.41	0.14	16.87	0.13	−0.67	0.31
CERC	−8.71318	37.78978	17.54	0.11	16.97	0.07	−1.34	0.17
LRIA	−8.7948	39.73153	17.58	0.07	16.76	0.08	−0.03	0.19
LEIR	−8.80533	39.72728	17.18	0.1	16.79	0.08	−0.41	0.17
ALCO	−8.87294	38.78532	17.44	0.16	16.73	0.09	−0.29	0.25
PMEL	−8.90345	38.57146	17.57	0.1	16.45	0.13	0.21	0.37
SAGR	−8.95964	37.02201	17.17	0.09	17.33	0.1	−1.57	0.23
ARRA	−8.9611	38.49276	17.4	0.08	16.55	0.07	0.05	0.15
AVIN	−9.07944	38.98289	17.87	0.26	16.82	0.21	0.29	0.41
CRAI	−9.13328	39.39418	17.63	0.09	16.63	0.07	−0.36	0.19
CRNH	−9.13541	39.40701	17.32	0.31	16.59	0.28	0.35	0.47
FCUL	−9.15687	38.75647	17.73	0.07	16.73	0.06	−1.86	0.16
IGP0	−9.15852	38.72603	16.91	0.12	15.94	0.11	−0.34	0.19
OALN	−9.18709	38.71056	17.93	0.25	16.67	0.19	0.09	0.49
PACO	−9.29491	38.69434	17.24	0.12	16.41	0.09	0.09	0.17
MAFR	−9.3261	38.93449	17.11	0.09	16.19	0.12	−0.04	0.16
CASC	−9.41852	38.69341	17.66	0.06	16.72	0.06	−0.18	0.12
IBIZ	1.44896	38.91125	20.49	0.12	16.17	0.09	−1.78	0.19
DENI	0.10366	38.83478	19.6	0.21	16.19	0.16	0.23	0.43

Note. E, N, and U represent the east, north, and up components of velocity, and σ_E, σ_N, and σ_U are the respective uncertainties, at the one sigma level, expressed in mm/yr.

segment, with one of the two possible fault planes oriented SW-NE and corresponding to left-lateral motion, as well as by some normal focal mechanisms. The SW end of the TASZ shows a more heterogeneous faulting style. In the Alboran Sea, between Gibraltar and the TASZ, a north–south swarm of earthquakes is recorded at depths of 60–100 km (Buforn et al., 1991, 1997; Mancilla et al., 2013). These earthquakes have been interpreted as tearing of the subducted slab (Lonergan & White, 1997). Recently, Santos-Bueno et al. (2019) showed that the focal mechanisms of these earthquakes do not correspond to downdip slip along a slab interface and rather interpreted them as faulting within ancient fractures of the subducted Jurassic-age oceanic lithosphere. South of the Alboran Sea, seismic activity is less well documented by current earthquake catalogs. The few focal mechanisms documented south of Gibraltar indicate strike-slip and normal faulting (Figure 3b).

4.2. Crustal Model PRISM3D

Figure 4 shows the 3-D *P* wave velocity and the crust-mantle boundary (Moho) surface provided by *PRISM3D*, a recent Earth structure model of the region (Arroucau et al., 2017; Civiero et al., 2018). To guide the analysis of the results, we define four main segments of the arc where we will focus our interpretation. From south to north along the arc, we define R1 (eastern Rif), R2 (Gibraltar domain), R3 (western Betics), and R4 (eastern Betics). PRISM3D merges previous models derived from a variety of data sets, including local and teleseismic body wave tomography, earthquake and ambient noise surface wave tomography, receiver function analysis, and active source experiments (see Table S3 for the complete list of models, type of study and depth range). The Moho surface was modeled using the probabilistic surface reconstruction algorithm of Bodin et al. (2012). PRISM3D relies on *EP*crust as initial model (Molinari & Morelli, 2011) and then updates it with recently published seismic observations from receiver function analysis and deep seismic sounding (Afilhado et al., 2008; Chevrot et al., 2014; Díaz & Gallart, 2009; Dündar et al., 2016; Mancilla & Diaz, 2015; Martínez-Loriente et al., 2014; Salah, 2014; Sallarès et al., 2011) (see Table S4 for the list of models and type of study). First-order features shown by the Moho topography are an eastward

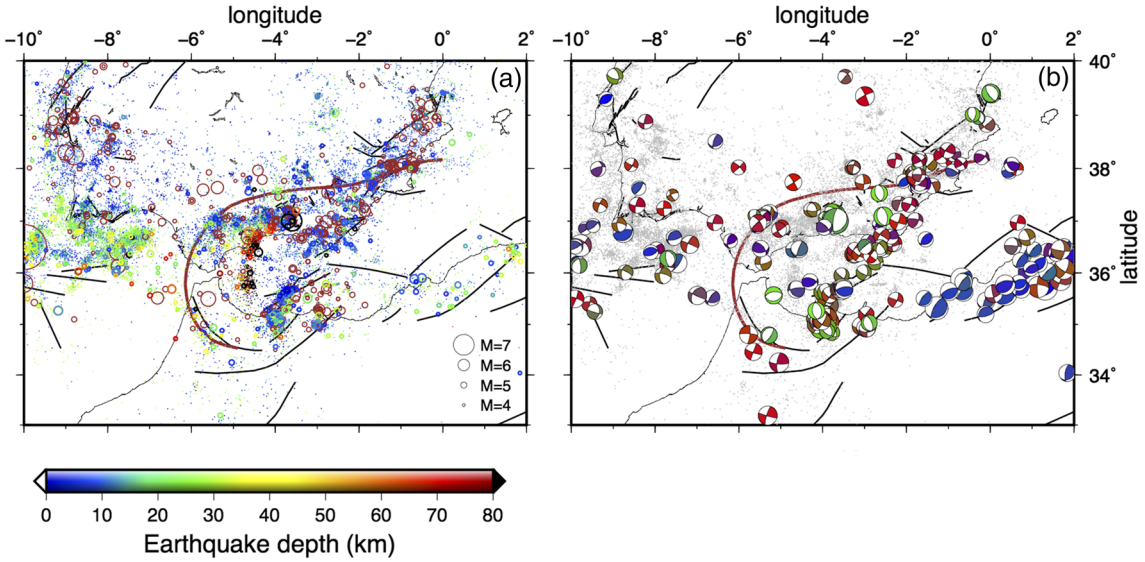

Figure 3. (a) Regional seismicity from the compilation of Custódio et al. (2016) (M > 4: circles, size corresponding to magnitude, color coded by depth, historical quakes plotted in brown; M < 4, 1996–2016: small dots, color coded by depth). (b) Focal mechanisms from Custódio et al. (2016) color coded according to the faulting style: Normal (green), strike slip (red), and reverse (blue). Gray dots in the background represent earthquake epicenters (same as in panel (a)).

dipping Moho below the Rif (R1) and a tight lateral bending of the downward dipping Moho around the Gibraltar Strait (R2). The latter divides the dipping Moho into a northern NE-SW oriented segment along Betics and a southern NW-SE segment in north Morocco (Figure 4). In the eastern Rif (R1) and western Betics (R3), we observe high crustal thicknesses (40–45 km), as well as sharp Moho gradients, in contrast with a shallower and flatter Moho south and east of the Rif, the eastern Betics (R4) and the Alboran Sea. The error associated with the Moho depth in the Gibraltar region in PRISM3D is high (2–4 km), which results from the locally high Moho gradients. Note that the strongly varying Moho depth below Gibraltar is a feature that is absent in the *EP*crust model of Molinari and Morelli (2011); however, it is clearly imaged by more recent studies, such that presented by Mancilla & Diaz (2015) and Díaz, Gil, et al. (2016). Similar to PRISM3D, the maximum crustal thicknesses in the model of Diaz, Gallart, and Carbonell (2016) are localized in the northern Rif and around Gibraltar Strait. Another deep Moho site is imaged by Diaz, Gallart, and Carbonell (2016) around the Sierra Nevada, whereas PRISM3D places the deeper Moho in southern Spain a bit further west. Moho depth observations in this region indicate some variability, which gives rise to different Moho reconstructions. Nevertheless, considering the statistical nature of the approach used to calculate the PRISM3D Moho interface, the Moho values and pattern agree quite well with the most recent seismic (Capella et al., 2017; Diaz, Gallart, & Carbonell, 2016; Mancilla et al., 2012; Mancilla & Diaz, 2015; El Moudnib et al., 2015; Thiebot & Gutscher, 2006) and petrological studies (Fullea et al., 2010).

4.3. Residual Topography

Residual topography is the topography observed once the isostatic component is filtered out. Hence, it may provide indications of a mantle dynamic support of topography. Dynamic topography can also be estimated from mantle convection models, by converting tomographic anomalies into thermal densities. Previous models indicate that the Iberia-Maghreb region has significant values of residual topography, with a generally positive uplift signal in the Gibraltar Arc System (Boschi et al., 2010; Faccenna et al., 2014; Faccenna & Becker, 2010). Here, we present a new residual topography map, computed as the difference between the observed and Airy isostatic topography, using the PRISM3D crustal model (Figure 5a, update from Faccenna et al., 2014 and T. Becker, personal communication, 2019). In particular, we used the crustal thickness estimate shown in Figure 4 and a constant lithospheric thickness of 82 km (Palomeras et al., 2017). We choose crustal (ρ_c) and mantle lithosphere (ρ_m) densities of 2,782 and 3,250 kg/m^3, respectively, and an

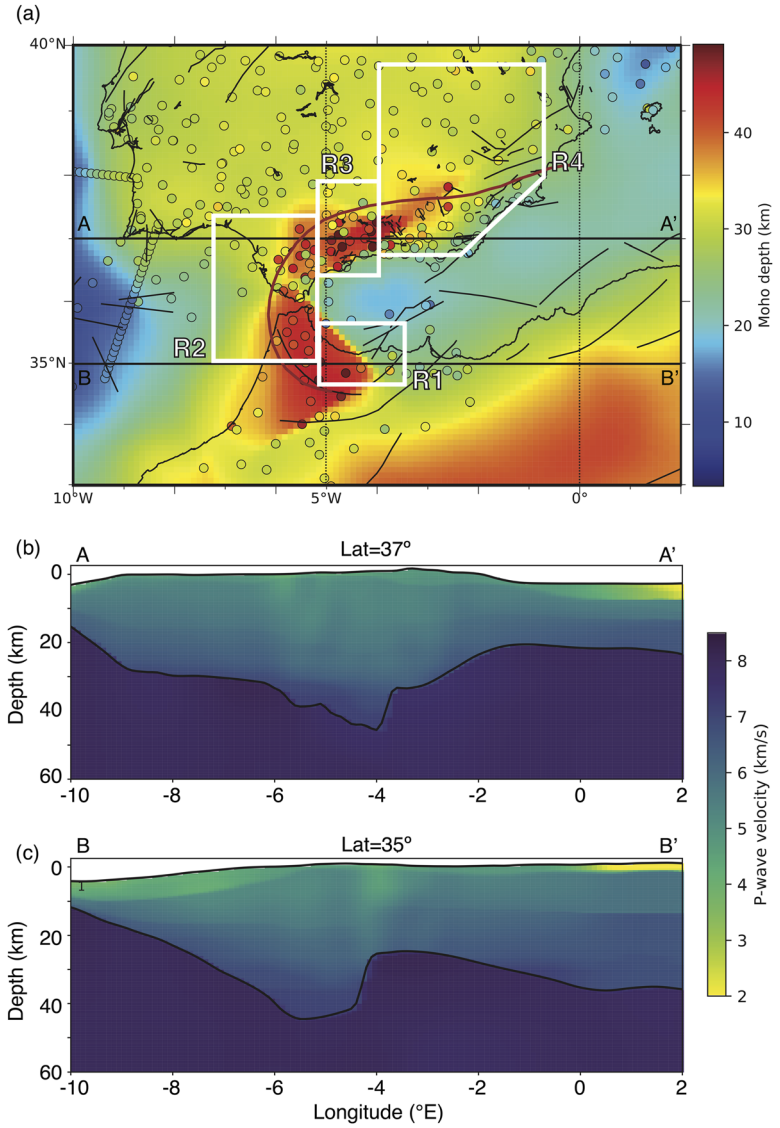

Figure 4. (a) PRISM3D Moho depth model from Arroucau et al. (2017), obtained by interpolation of receiver functions and deep seismic sounding results. Small colored circles show the Moho depth values observed. The regions discussed in the text are identified in white: R1 (eastern Rif), R2 (Gibraltar domain), R3 (western Betics) and R4 (eastern Betics). (b, c) WE cross sections through the V_P structure of PRISM3D at latitudes of 37°N, cutting through the Betics (b), and 35°N, cutting through the Rif (c). An eastward dipping Moho is observed in both profiles, below the eastern Rif (R1) and the western Betics (R3).

asthenospheric density (ρ_a) of 3178 kg/m^3. Under these assumptions, the Airy residual estimate reveals that the topography of the Gibraltar Arc System is not fully compensated by crustal isostasy, indicating that at least part of the topography could be associated with the mantle dynamic processes. However, we have to keep in mind that the mantle contribution to topography may also result from lithospheric density heterogeneities, which are not accounted for in our modeling. Figure 5a shows that a negative residual topography is observed in the proximity of the Gibraltar Arc (R1-R3), with a maximum amplitude of ~−1,300 m in the Rif. In contrast, a positive signal is obtained in the rest of the region, reaching amplitudes of 1000 m south and east of the Rif, as well as in the eastern Betics (R4). These new results indicate that the Gibraltar Arc region stands lower than what would be expected from crustal isostatic balance, whereas the regions south and east of the Rif and the eastern Betics (R4) stand higher than if

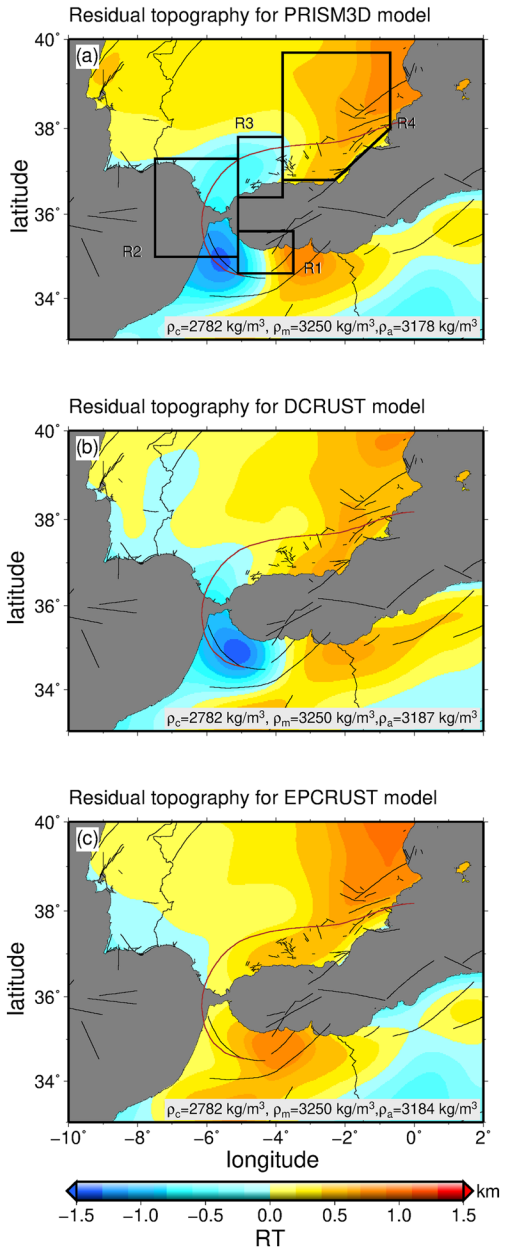

Figure 5. Residual topography computed using the (a) the PRISM3D crustal model shown in Figure 4; (b) the crustal model DCRUST, a combination of the model from Diaz, Gallart, and Carbonell (2016) and CRUST1.0 (Laske et al., 2013); and (c) the EPCRUST crustal model (Molinari & Morelli, 2011) (T. Becker, personal communication); ρ_c, ρ_m, and ρ_a used in the computation are indicated at the bottom of each panel. The reference mean ridge level is $t_0 = -2.6$ km (Carlson & Johnson, 1994). The regions discussed in the text are identified in panel (a). The strongly negative values of residual topography around Gibraltar observed both in (a) and (b) indicate that the Gibraltar region should stand higher than the observed elevation if it were in isostatic balance. The positive residual topography in the eastern Betics (R4) and east of the Rif is observed in all the panels and means that these regions should stand at a lower elevation relative to the actual topography if they were isostatically balanced.

isostatically balanced. We also compute two additional residual topography solutions, one using the regional model of Diaz, Gallart, and Carbonell (2016) combined with the global crustal model CRUST1.0 (Laske et al., 2013) (hereafter referred to DCRUST) (Figure 5b), and the other using the European *EP*crust model (Molinari & Morelli, 2011) (Figure 5c). We show the difference in residual topography between these models in supporting information Figure S3. The first solution shows similar results (Figures 6b and S3a), while the latter—which lacks the observed lateral variability of the Moho near Gibraltar—has values of residual topography close to zero in the Gibraltar Strait region (Figures 6c and S3b).

In the next section we will compare the residual component of the topography with the crustal and mantle structure, seismicity and volcanism of the region to explore if the topography may be related to stresses resulting from mantle dynamics.

4.4. Mantle Model IBEM-P18

Civiero et al. (2018) combined *P* wave travel time data sets from all available regional seismic deployments from the Pyrenees, in the NE, to northwest Morocco and Canaries, in the SW, to provide a new high-resolution tomographic model of the Iberia-Maghreb region (*IBEM-P18*), extending from ~70- to 800-km depth. The imaged seismic structure confirms the main large-scale features documented by previous tomographic models (e.g., Bezada et al., 2013; Bonnin et al., 2014; Chevrot et al., 2014; Monna et al., 2013; Figure S4). However, the larger number of stations used, and resulting broader areal coverage of the data set, increased the depth range of the tomographic imaging, thus allowing us to discuss the relationship between anomalies in the upper and topmost lower mantle. Furthermore, the introduction of PRISM3D as a starting model allowed us to minimize the contributions to the travel-time anomalies from unresolved crustal structure, thus improving the resolution and robustness of the mantle model. IBEM-P18 images a prominent fast body ($\delta V_P > 0.3$ km/s in its center) below the Alboran Sea, Betics, and Rif, which extends from ~200-km depth down to the base of the mantle transition zone (Figure 6). The fast anomaly is arcuate in shape, concave on the Alboran Sea side down to ~400-km depth and dips steeply downward. This structure is surrounded by slow seismic anomalies ($\delta V_P \approx -0.2$ km/s) in the upper mantle (Figure 6), suggesting that the fast body below the Alboran Sea interacts with the surrounding hot mantle (Civiero et al., 2018, 2019). Other small-scale (~100 km of diameter at lithospheric depths) high-velocity anomalies are imaged below the eastern Rif (R1) and the western Betics (R3). The first extends downward from the surface through the upper mantle, and the latter from ~100 km depth downward. These features are imaged as laterally connected to the strong high-velocity anomaly below the Alboran Sea, evidencing the continuity of the lithospheric piece down to mantle transition zone levels.

Figure 7 shows a resolution test beyond those shown in Civiero et al. (2018) aimed to evaluating if the connectivity of the small-scale uppermost mantle structure below Betics and Rif with the main high-velocity anomaly in the upper mantle is the result of vertical smearing. We place three discrete spikes ($\delta V_P = 0.6$ km/s, diameter = ~100 km) along each profile AA′ and BB′ at ~50-km depth. The recovered images are overall well retrieved and show that the anomalies remain restricted to a relatively shallow depth

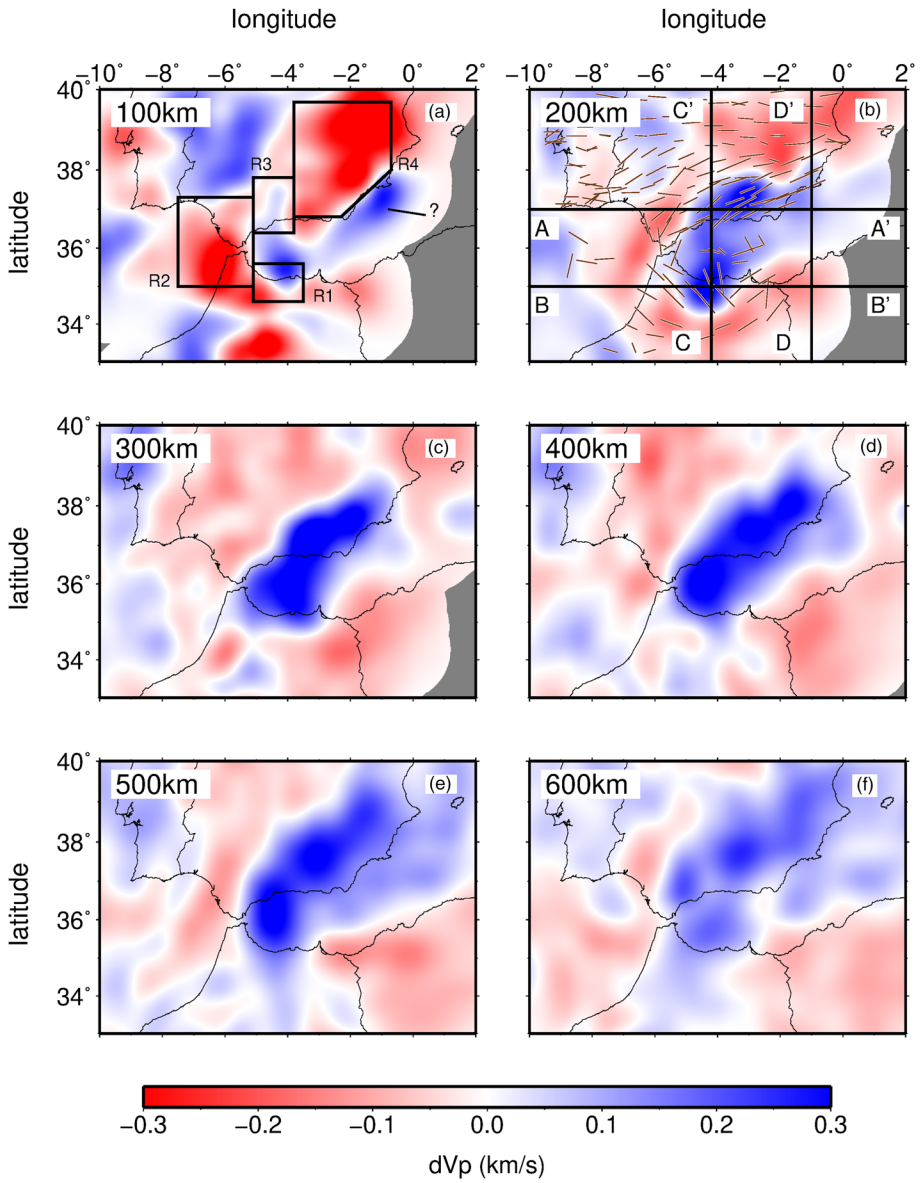

Figure 6. (a–f) Depth slices through the tomographic *P* wave model IBEM-P18 (damping = 5, smoothing = 5) of Civiero et al. (2018) at depths between 100 and 600 km. The velocities are relative to the 1-D laterally averaged depth-dependent version of PRISM3D and LNLL models (Simmons et al., 2012), used as a reference model (see Civiero et al., 2018, for details). The *SKS* splitting measurements from Díaz et al. (2010, 2015) and Díaz and Gallart (2014) are plotted over the panel (b) with brown bars, whose orientation is aligned with the fast direction. The regions discussed in the text are identified in panel (a). Profiles AA′ and BB′ in panel (b) are referred to Figure 8. Profiles CC′ and DD′ are referred to Figure S5. Note the high-velocity body below the Alboran Sea surrounded by low-velocity anomalies in the upper mantle below the external Betics and Rif.

level although a small amount of smearing occurs along rays. These results suggest that the connection between the small-scale features R1 and R3 with the high-velocity body centered below Alboran Sea is a robust feature of the tomographic model.

5. Discussion

Competing evolutionary models have been proposed to explain the present-day tectonics of the Gibraltar Arc System. A group of studies attributes the extension observed in the Alboran basin and the formation of the

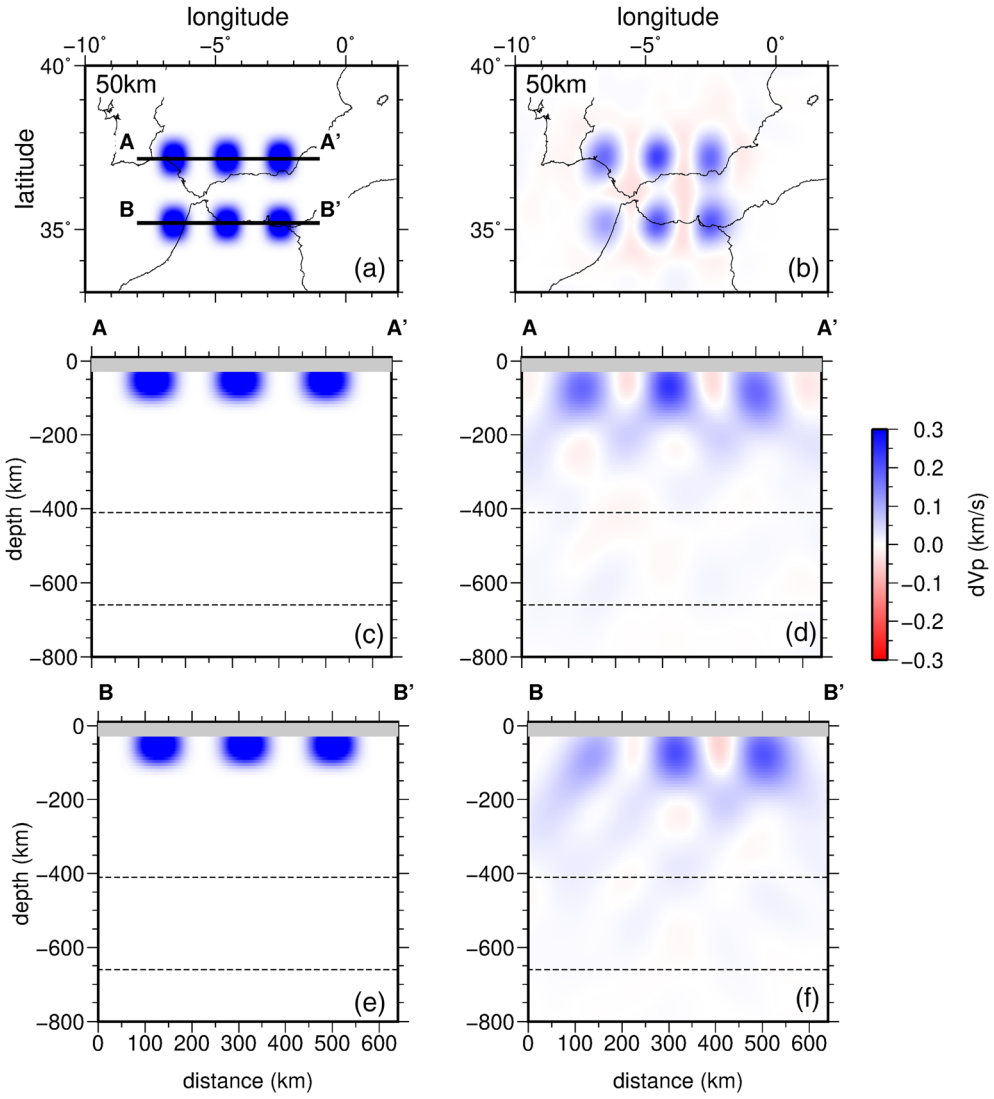

Figure 7. Spike resolution test for the IBEM-P18 model, using a layer of six high-velocity anomalies of ~100 km width and 0.6 km/s in amplitude separated by regions of zero perturbation. (a) Input model at 50 km depth. (b) Output *P* wave velocity structure at 50-km depth. (c, e) Vertical cross sections AA′ (c) and BB′ (e) through the input model (orientations of the profiles are shown in depth slice a) and are the same of profiles AA′ and BB′ in Figure 4. (d, f) vertical cross sections AA′ (d) and BB′ (f) through the recovered model. The same raypaths and inversion parameters that are used in the inversion of the observations are used here. Crustal structure is gray shaded. Despite some smearing along the oblique ray paths, the anomalies are well retrieved. Note that the resolution of the western anomaly in profile BB′ is weaker as the location is almost entirely offshore.

Betic-Rif cordillera to delamination (e.g., Calvert et al., 2000; Platt et al., 1998; Seber et al., 1996) and/or to convective removal of the Alboran underlying lithosphere (e.g., Houseman, 1996; Platt & Vissers, 1989). Other models propose that the formation of the Gibraltar Arc System can be explained by subduction rollback, with slab break-off (e.g., Blanco & Spakman, 1993; Zeck, 1996) or without slab break-off (e.g., Faccenna et al., 2004; Gutscher et al., 2002; Lonergan & White, 1997; Royden, 1993), driven by the negative buoyancy of the subducting slab and accompanied by extension in the backarc. All the hypothesized processes require the sinking of negatively buoyant lithosphere and the simultaneous rising of positively buoyant sublithospheric mantle. However, these models are incompatible with each other and predict different key observations.

A robust model of the Gibraltar Arc System needs to be consistent with all the existing observations. Here, we integrate seismic, tomographic, and geodetic data to discuss the different proposed geodynamic models.

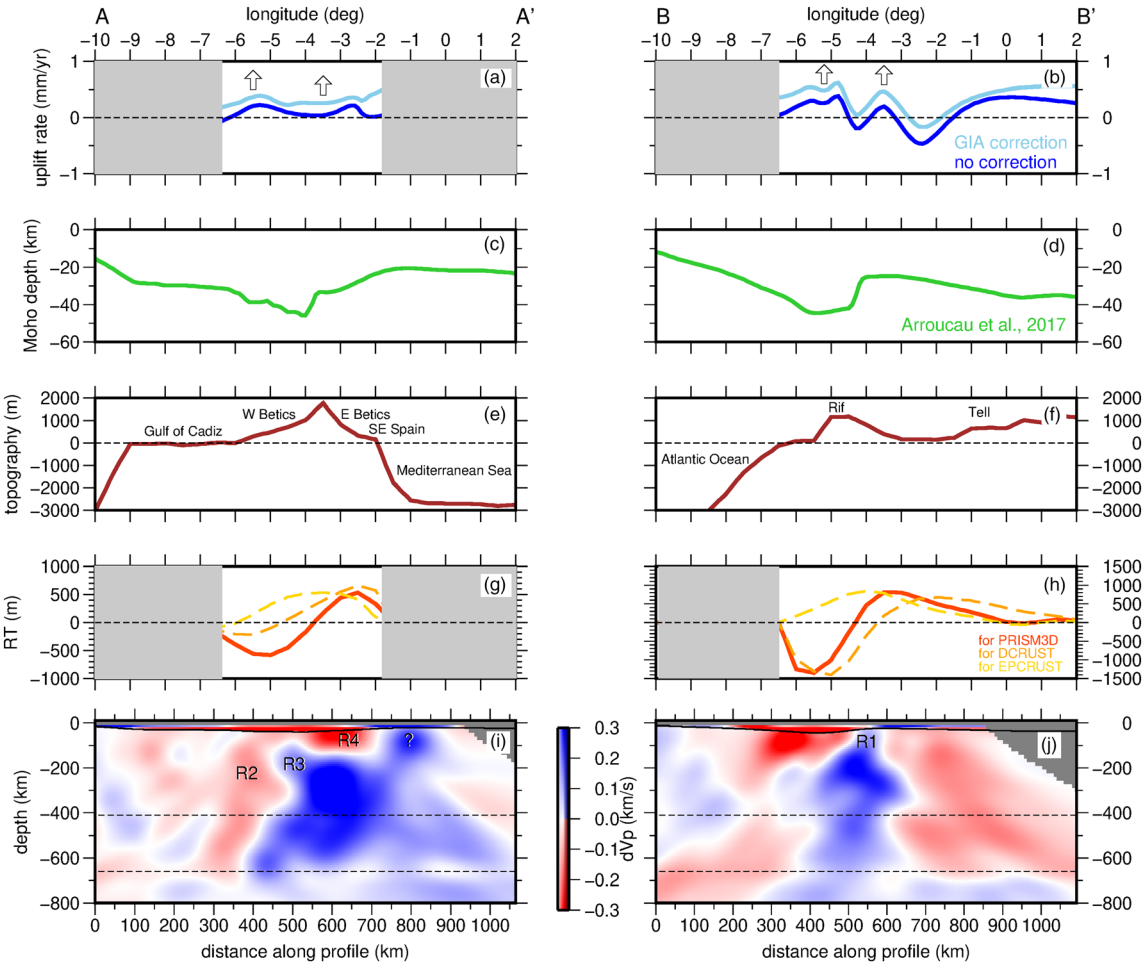

Figure 8. Cross sections comparing geodetic vertical velocity, Moho depth, topography, and mantle structure along two representative EW profiles through the Betics (AA′) and the Rif (BB′). The orientation of the profiles is shown in Figure 6b and is the same as those in Figure 4. (a, b) Smoothed vertical GPS velocities without (dark blue line) and with GIA correction model ICE-5G (light blue line) applied. The sea domains are masked in gray due to the lack of data. (c, d) Moho depth from Arroucau et al. (2017). (e, f) Topography profiles (expressed in m) from SRTM30+ (Smith & Sandwell, 1997). (g, h) Residual topography (expressed in m) using the PRISM3D (red line), DCRUST (orange), and EPCRUST (yellow line) crustal thickness. The sea domains are masked in gray. (i, j) Seismic mantle structure from the *P* wave tomographic model of Civiero et al. (2018). The regions discussed in the text are identified in each profile. Regions with no piercing points are shaded gray.

To assist our analysis, we show in Figure 8 two cross-sections through the Betics and Rif respectively, as imaged by the IBEM-P18 tomographic model, together with the vertical GPS velocities, the Moho depth, and the actual and residual topography, along the same profiles. Figure S5 shows another two cross sections, CC′ and DD′, along profiles perpendicular to AA′ and BB′, respectively.

Our recent tomographic model IBEM-P18, combined with the PRISM3D crustal model, images the structure below the Gibraltar Arc System at high resolution, on the order of 100–150 km, allowing us to interpret with confidence the seismic anomalies from the surface down to the mantle transition zone (Civiero et al., 2018). Below the western Betics (R3, Figure 8i) and eastern Rif (R1, Figure 8j), the high-velocity mantle anomalies appear to be relatively continuous from lithospheric depths down through the transition zone. Where the imaged high-velocity structure is continuous, the calculated residual topography values (considering the PRISM3D crustal model) are negative or close to 0, suggesting that the lithosphere is still deflected downward (Figures 4 and 8g and 8h). This does not seem to be the case below the eastern Betics (R4), where prominent low-velocity anomalies are imaged in the uppermost mantle (down to ~150-km depth) and positive residual topography values are found, suggesting that the lithospheric body is entirely disconnected from the surface (Figures 8g and 8i). The computed PRISM3D Moho depths are deeper below R1 and R3 where

continuous high-velocity anomalies are imaged, and shallower eastward, following the geometry of the high-velocity-low-velocity interface (Figures 4 and 8). In addition, the anisotropic mantle fabric derived from *SKS* splitting analyses shows arc-parallel fast directions, overlapping with the low-velocity structure imaged around the fast anomaly (e.g., Buontempo et al., 2008; Díaz et al., 2010; Miller et al., 2013) (Figure 6b).

These observations together support the existence of a subducting slab and cannot be readily explained by lithospheric delamination or foundering models. The significant vertical extent of the high-velocity anomaly is unlikely to result from delamination alone, which would have indicated a much smaller amount of sinking material (Bonnin et al., 2014). In addition, anisotropic fast directions oriented radially are required to explain the asthenospheric mantle that replaces the removed lithosphere (Buontempo et al., 2008; Díaz et al., 2010). The *SKS* splitting results in Figure 6b show, however, that the flow is oriented more or less tangentially to the Alboran Sea domain. In turn, convective removal of the lithosphere would generate more rounded and sparse anomalies detached from the surface. Such models would produce a more symmetric arc system and not a horseshoe-arc-shaped mountain belt with an accretionary wedge to the west (Gutscher et al., 2002; Schellart & Lister, 2004). Furthermore, the distribution of calc-alkaline volcanism in the eastern Betics, Morocco and Alboran Sea dating from the Miocene, between 25 and 5 Ma, require the transport and circulation of fluids from the surface to high depths (80–120 km) only possible in a subduction environment (e.g., Bosch et al., 2014; Duggen et al., 2005; Faccenna et al., 2004; Gill et al., 2004; Lustrino et al., 2011) (Figure 1). According to this interpretation, a subducted piece of lithosphere is the only possible explanation for the deep-focus earthquakes observed below the Alboran Sea and Granada region (e.g., Bezada & Humphreys, 2012; Buforn et al., 2011) (Figure 3). In light of these observations, we conclude that a subvertical E dipping subducted slab below the Gibraltar Arc System, extending through the upper mantle down to the upper-lower mantle boundary, is the only model supported by the integrated data set.

5.1. Has the Gibraltar Slab Broken off?

It is currently debated whether the slab is still attached to the surface and whether the subduction zone remains active (Duarte et al., 2013; Gutscher et al., 2012; Iribarren et al., 2007; Spakman & Wortel, 2004; Zitellini et al., 2009). Some authors have proposed that the subducted slab has fully broken off and is no longer influencing the geodynamics of the region (e.g., Cunha et al., 2012; Duggen et al., 2003), whereas others have suggested that it is still entirely attached to the surface (e.g., Alpert et al., 2013). Other recent studies agree that only residual slab segments (below the Rif and the Betics) are still connected to the surface or in the process of detaching (e.g., Carballo et al., 2015; Garcia-Castellanos & Villaseñor, 2011; Levander et al., 2014; Mancilla & Diaz, 2015; Palomeras et al., 2014; Spakman et al., 2018; Thurner et al., 2014; Vernant et al., 2010). According to our integrated analysis, the subducted slab appears to be indeed segmented, with a few portions still attached to the surface or in the process of detaching below the eastern Rif (R1) and the western Betics (R3), while a wide portion of the slab seems to have fully broken off below the eastern Betics (R4). The TASZ, the present-day eastern limit of the overriding Alboran block (Neres et al., 2016), seems to accommodate the differential motion between, on one side, the west Alboran, western Betics and Rif crust, which are partially still connected to the slab and, on the other side, the eastern Alboran crust and eastern Betics, which are no longer connected to the slab.

The idea that the slab is still attached to the surface (or detaching from the crust) in the eastern Rif (R1) and the western Betics (R3) explains: (i) the deep Moho plunging from depths of ~10 km up to more than 40 km; (ii) the vertical continuity of the tomographically imaged fast anomaly down to the mantle transition zone; and (iii) the negative (or around 0) residual topography, indicating that the Gibraltar Strait region stands lower than what would be expected from isostatic balance. The connection of the slab to the surface below the eastern Rif (R1) is further supported by controlled-source and natural seismicity surveys (Díaz, Gil, et al., 2016), surface wave tomography (Palomeras et al., 2014, 2017), and gravity studies (Petit et al., 2015). To the north, in the western Betics (R3), the evidence that a segment of the slab is still attached to the surface, or in the process of breaking off, agrees well with previous tomographic models (Levander et al., 2014; Palomeras et al., 2014; Spakman & Wortel, 2004) and receiver functions studies (Thurner et al., 2014).

The scenario is different around the Gibraltar Strait (R2), where few observations indicate that the crust is slightly thinner than that of neighbor domains (Figure 4), the IBEM-P18 tomographic images show a prominent low-velocity body, which extends down through the upper mantle (Figure 6) and the residual topography is negative (Figure 5). This short segment thus appears to be either fully detached or currently detaching

from the surface, in agreement with the recent model of Thurner et al. (2014), and forming a small slab window. The formation of such subduction window may have been aided by the continued plate convergence between Nubia and Eurasia since post-Miocene times, which seems to have tightly bent the subducted slab around a vertical axis centered near the Gibraltar Strait (Mattei et al., 2006), thus facilitating the detachment of this portion of the slab. Strongly negative dilatational rates around Gibraltar (i.e., shortening) indicate that the plate convergence is still significantly driving deformation here (Figure 2). The ongoing compression is likely to induce the enlargement of the subduction window with time. This suggests that the topography may have not yet recovered its isostatic equilibrium position explaining why the residual topography is still negative. One would expect that only once the slab is fully detached from the plates at the surface the residual topography values would become neutral, or even positive in case of rebound.

The existence of a detached slab in the eastern Betics (R4) is also supported by current observations, namely, (i) a substantially shallow Moho (Sierra Nevada excluded), becoming even shallower than in inner stable Iberia; (ii) a strong low-velocity anomaly (down to ~150 km depth), as tomographically imaged by the IBEM-P18 model; and (iii) the residual topography gradually becoming positive, which indicate that the eastern end of the arc stands higher than would be expected in a situation of crustal isostatic equilibrium. These pieces of evidence suggest that the slab is progressively tearing below the eastern Betics (R4), in consequence of the subduction of continental Iberian crust (e.g., Duggen et al., 2004; Mancilla & Diaz, 2015). The present-day tearing of the Iberian lithosphere has been proposed to be occurring along a near-vertical EW striking STEP fault that is expressed in the crust as a positive flower structure, imaged by receiver functions (Mancilla et al., 2018).

In SE Spain, the data allow us to speculate on a remnant segment of the slab. Similar to the previous tomographic model of Palomeras et al. (2014), IBEM-P18 images a small high-velocity anomaly, which extends offshore (Figures 6 and 7). This anomaly appears continuous from the crust to transition zone depths and may indicate a small remnant portion of the subducted lithosphere of the Balearic margin that is still attached to the surface. However, the resolution in this part of the tomographic model is limited (Civiero et al., 2018) and better seismic coverage is needed to image clearly the finest details of the structure.

5.2. Is the Gibraltar Subduction Zone Still Active?

The subducted Gibraltar slab does not seem to be continuously connected to the surface over the entire length of the arc. Several segments of the slab show signs of slab break off and are characterized by slab windows. This suggests that the slab is detaching from the surface and that the subduction system is reaching its final stages of evolution, as a result of the entering of continental blocks in the subduction zone (Figure 9). The remaining question is whether the slab segments that are still attached to the surface, to the west, can transmit stresses efficiently to the surface plates, causing seismotectonic deformation and eventual facilitating the propagation of the arc to the west, where some oceanic lithosphere is still available to subduct.

The observed negative residual topography in the Rif, the Gibraltar domain and the western Betics (R1-R3) indicates that the surface topography is deflected downward, likely in result of the action of slab pull forces. However, the GPS vertical data suggests that portions of the arc's surface are presently moving upward (uplift, see Figures 2 and 8). A hypothesis that could explain these apparently contradictory observations is that the slab pull force is decreasing as the result of a progressive (viscous) detachment of the slab and is losing its capacity to propagate stresses to the surface efficiently, causing its uplift (see discussions in Gutscher et al., 2012; Neres et al., 2016; Serpelloni et al., 2013; Stich et al., 2006). The observed uplift would, therefore, result from the progressive restoration of isostatic equilibrium. Such interpretation suggests that the subduction interface may not be active, at least as one would expect from a classical subduction system. This is in agreement with the lack of instrumental earthquakes along the subduction interface. Furthermore, a recent study found several focal mechanisms within the subducted plate, at 60- to 100-km depth, east of Gibraltar, without a clear relation with downdip stresses and suggested that the process of subduction has come to a halt or slowed down significantly (Santos-Bueno et al., 2019).

Below the eastern Betics (R4), the surface stands higher than what would be expected from isostatic equilibrium and, in accordance, the GPS data depicts mostly upward vertical crustal motion. This region is also characterized by a shallow lithosphere-asthenosphere boundary, compared with the surrounding regions

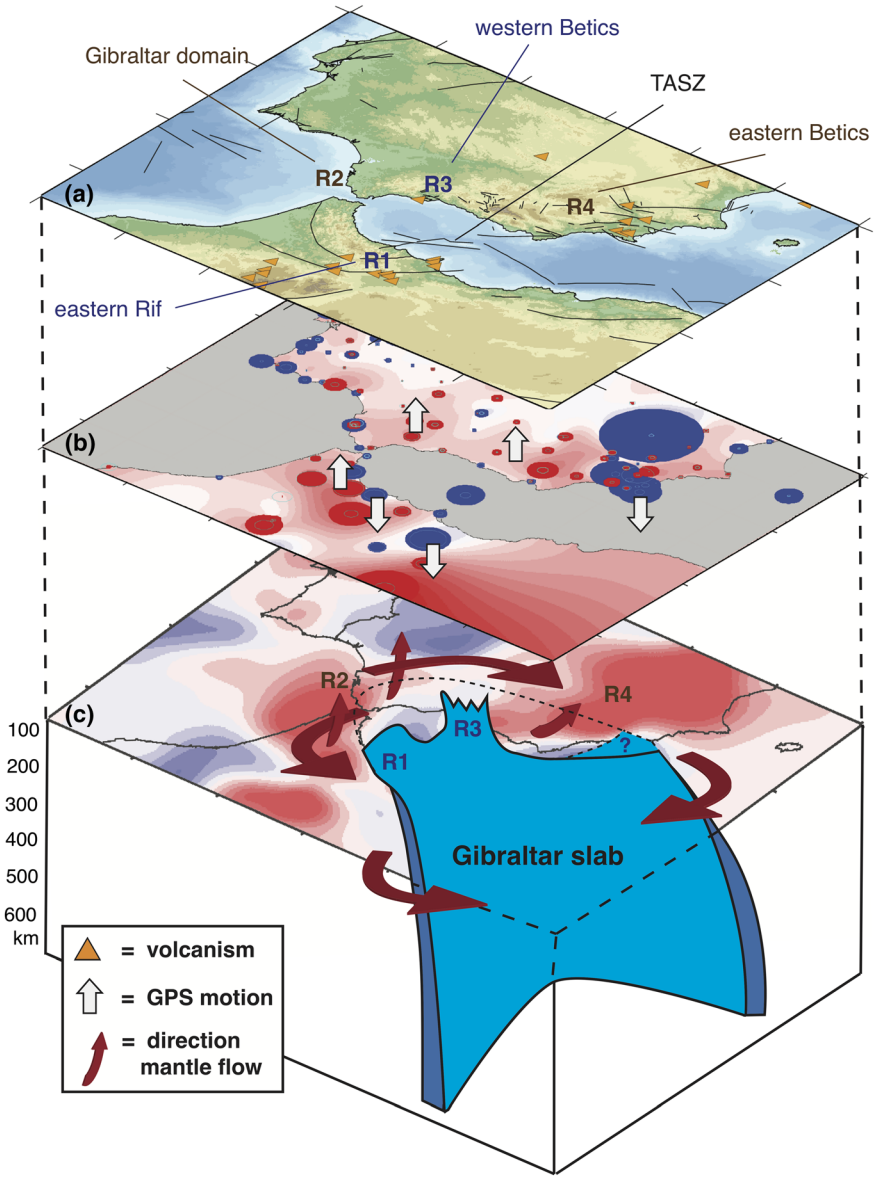

Figure 9. Schematic cartoon of the proposed geometry and dynamics of the Gibraltar slab. (a) Topography of the Gibraltar arc system. The regions of the arc discussed in the text are indicated in blue (R1 and R3: Segments still attached to the surface or in the process of detaching) and brown (R2 and R4: Segments of the arc detached). The volcanism is shown with orange triangles. The TASZ and other major faults are indicated in black. (b) The vertical GPS motion with white arrows indicating the most significant regions of uplift and subsidence. (c) The simplified 3-D geometry of the slab below the IBEM-P18 model at 100-km depth. The red arrows indicate the mantle flow pushing asthenospheric material toward the lateral edges of the slab and through the slab windows.

(Palomeras et al., 2014, 2017), and a dominantly positive dilatational strain field, in agreement with dominantly trans-tensional and some normal crustal earthquake focal mechanisms (Figures 2b and 3). Such evidences suggest that the slab has detached here, with the opening of a slab window and the inflow of asthenospheric mantle (Carballo et al., 2015; Faccenna et al., 2011; Fullea et al., 2010; Molina-Aguilera et al., 2019; Palomeras et al., 2014, 2017). Numerical and laboratory studies (Funiciello et al., 2006; Li & Ribe, 2012; Piromallo et al., 2006; Schellart, 2008; Stegman et al., 2006; Strak & Schellart, 2014) show that narrow rolling-back slabs induce strong quasi-toroidal mantle flow around their lateral edges. We suggest that this mantle return flow may still be active around the Gibraltar Arc, as evidenced by *SKS* splitting results (e.g., Díaz et al., 2010). Although subduction is currently very slow or stopped, the slab may be still

moving (and steepening) in the mantle as a result of its negative buoyancy, thus forcing subslab material to flow around its lateral edges with an upward flow component, emerging below the eastern Betics (R4) and east of the Rif. The impingement of vertical mantle flow forces the upward dynamic bending of the lithosphere and associated positive vertical topographic motion (Figure 9). Such mantle inflow is likely to have weakened the lithosphere, eventually facilitating the development of the TASZ. The very active seismicity along the TASZ is in good agreement with the high strain rates observed in the region from GPS data. In addition, the transtensional faulting regime indicated by focal mechanisms along the TASZ is consistent with the observed dilatational field (Figure 3).

The process of lateral slab disruption and window formation may have initiated in the late Miocene and to be continuing at the present (Faccenna et al., 2004). The overall uplift has been proposed to be responsible for the closure of the gateways between the Mediterranean and the Atlantic ~5.8 Ma ago, causing the Messinian salinity crisis (Duggen et al., 2003; Garcia-Castellanos & Villaseñor, 2011; Krijgsman et al., 1999). The intraplate calc-alkaline volcanic fields found since ~5 Ma around the lateral edges of the slab in southern Spain and northeast Morocco (Duggen et al., 2005; Lustrino & Wilson, 2007; Maury et al., 2000) and the thermobarometric analysis of basalts (Thurner et al., 2014) provide further evidence for the existence of this upwelling system, where asthenospheric mantle fills the detached portions of the lithospheric slab and generates partial melting at depths of 40–80 km.

The regional convergence between Iberia and Africa can contribute significantly to the observed folding and uplift with the consequent increase of the emerged areas in the Betic-Rif chain from late Tortonian onward (Braga et al., 2003; Iribarren et al., 2009; Sanz de Galdeano & Alfaro, 2004). As shown in Figure 8, the uplifted region around Gibraltar (R1–R3) shows a clear match with the high crustal thickness distribution below. In the Rif, tectonic deformation occurs at local scale. Recently, Spakman et al. (2018) proposed that the slab-edge indentation along the African margin due to mantle-resisted slab dragging provides a straightforward explanation for the local crustal thickening of the Rif. This shortening would produce inter-seismic strain accumulation that would be expressed at the surface by local uplift. Such process would explain the few southwestward GPS velocities of the northern Rif (in a Nubian-fixed reference frame; see Figure 2a). This observation is in agreement with previous geodetic studies that have interpreted the Rif subblock behavior as an evidence that a segment of the slab is still attached to the surface, and rolling back southwestward, below this region, producing local shortening at crustal levels (e.g., Pérouse et al., 2010; Vernant et al., 2010). However, the observed low rates of horizontal GPS rates in the northern Rif (~1 mm/yr) suggest that, if such process is indeed occurring, it should be significantly less active in the present day.

Additional geophysical studies combined with numerical modeling will allow testing different evolutionary scenarios that take into account the 3-D structure of the slab and the various driving forces at work in the region.

6. Conclusions

In this work, we presented a new dense GPS data set that provides a detailed view of the horizontal and vertical surface motion in the Gibraltar Arc System. We also computed residual topography using different crustal models available in literature. We then comparatively analyze these results together with up-to-date Moho depth estimates, mantle structure images, and seismicity of the region. The integration of these observations allows us to provide a conclusive understanding of the highly debated evolution of the region, validating some previously published hypotheses and adding new fresh insights on the geometry and dynamics of the arc. According to our interpretation, the Gibraltar subduction interface appears to be no longer active as a continuous arc. In agreement with previous findings, the slab appears clearly detached from the surface beneath the eastern Betics as a result of slab tearing. However, it seems to be still locally attached to the surface (or has just recently detached) in the eastern Rif and in the western Betics. The remaining slab pull on the subducted continental margin is depressing the Moho downward. A young slab window is forming around the Gibraltar Strait under the ongoing compression between the African and Eurasian plates. However, the negative residual topography suggests that the isostatic equilibrium has not been reached yet.

Finally, we propose that most of the uplift observed in the Betic-Rif chain is due to inflow of asthenospheric mantle material, which replaces the detached lithosphere at shallow depths and pushes the surface upward.

The Africa-Eurasia convergence and the slab-edge indentantion into African continental lithosphere may additionally contribute to the uplift in NW Morocco, where the slab is still attached to the surface.

Acknowledgments
The authors would like to thank the Editor, Paul Tregoning, the Associate Editor, Fabio Capitanio, Claudia Piromallo, and an anonymous reviewer for constructive comments that improved the clarity of the paper. We thank all private and public institutions providing free access to GPS data. Morocco Regional GPS Surveys (1999: doi:10.7283/T589143S; 2001: doi:10.7283/T5W09456; 2002: doi:10.7283/T5R78CGX; 2004: doi:10.7283/T50R9MMB; 2006: doi:10.7283/T54J0CBM) were provided by the UNAVCO Facility with support from the National Science Foundation (NSF) and National Aeronautics and Space Administration (NASA) under NSF Cooperative Agreement EAR-0735156. The mantle IBEM-P18 model is available online from the IRIS Earth Model Collaboration (http://ds.iris.edu/ds/products/emc-near-p15near-s16). We also thank Thorsten Becker, Daniel Stich, and Luis Matias for fruitful discussions. C. C. was supported by the Project SPIDER (PTDC/GEOFIQ/2590/2014) from the Fundação para a Ciência e a Tecnologia, by the Science Foundation Ireland, the Geological Survey of Ireland, and the Marine Institute (Grants 13/CDA/2192 and 16/IA/4598). J. D. and S. C. acknowledge funding from the FCT through the project UIDB/50019/2020-IDL. J. D. further acknowledges an exploratory project Grant Ref. IF/00702/2015. C. F. is supported by Dipartimento di Eccellenza. GMT software (Wessel & Smith, 1995) was used to plot Figures 1–3 and 5–9. Obspy software was used to plot Figure 4 (Megies et al., 2011).

References

Abidin, H. Z., Andreas, H., Djaja, R., Darmawan, D., & Gamal, M. (2008). Land subsidence characteristics of Jakarta between 1997 and 2005, as estimated using GPS surveys. *GPS Solutions*, *12*(1), 23–32. https://doi.org/10.1007/s10291-007-0061-0

Afilhado, A., Matias, L., Shiobara, H., Hirn, A., Mendes-Victor, L., & Shimamura, H. (2008). From unthinned continent to ocean: The deep structure of the West Iberia passive continental margin at 38°N. *Tectonophysics*, *458*(1–4), 9–50. https://doi.org/10.1016/j.tecto.2008.03.002

Alpert, L. A., Miller, M. S., Becker, T. W., & Allam, A. A. (2013). Structure beneath the Alboran from geodynamic flow models and seismic anisotropy. *Journal of Geophysical Research, Solid Earth*, *118*(8), 4265–4277. https://doi.org/10.1002/jgrb.50309

Altamimi, Z., Métivier, L., & Collilieux, X. (2012). ITRF2008 plate motion model. *Journal of Geophysical Research, Solid Earth*, *117*(7), 1–14. https://doi.org/10.1029/2011JB008930

Altamimi, Z., Collilieux, X., & Metivier, L. (2011). ITRF2008: An improved solution of the international terrestrial reference frame. *Journal of Geodesy*, *85*(8), 457–473. https://doi.org/10.1007/s00190-011-0444-4

Arroucau, P., Custódio, S., Civiero, C., Dias, N. A., & Silveira, G. (2017). PRISM3D: A preliminary 3D reference seismic model of the crust and upper mantle beneath Iberia. *In 19th EGU General Assembly, EGU2017, proceedings from the conference held 23–28 April, 2017* (Vol. 19, p. 16801). Vienna, Austria: Geophysical Research Abstracts.

Basili, R., Kastelic, V., Demircioglu, M. B., Garcia Moreno, D., Nemser, E. S., Petricca, P., et al. (2013). The European Database of Seismogenic Faults (EDSF) compiled in the framework of the Project SHARE, http://diss.rm.ingv.it/share-edsf/. Retrieved June 7, 2019, from http://www.seismofaults.eu/index.php/services/edsf13-services

Becker, M., Zerbini, S., Baker, T., & Bu, B. (2002). Assessment of height variations by GPS at Mediterranean and Black Sea coast tide gauges from the SELF projects. *Global and Planetary Change*, *34*, 5–35. https://doi.org/10.1016/s0921-8181(02)00103-0

Bezada, M. J., & Humphreys, E. D. (2012). Contrasting rupture processes during the April 11, 2010 deep-focus earthquake beneath Granada, Spain. *Earth and Planetary Science Letters*, *353–354*, 38–46. https://doi.org/10.1016/j.epsl.2012.08.001

Bezada, M. J., Humphreys, E. D., Toomey, D. R., Harnafi, M., Dávila, J. M., & Gallart, J. (2013). Evidence for slab rollback in westernmost Mediterranean from improved upper mantle imaging. *Earth and Planetary Science Letters*, *368*, 51–60. https://doi.org/10.1016/j.epsl.2013.02.024

Bird, P. (2003). An updated digital model of plate boundaries. *Geochemistry, Geophysics, Geosystems*, *4*(3). https://doi.org/10.1029/2001GC000252

Blanco, M. J., & Spakman, W. (1993). The P-wave velocity structure of the mantle below the Iberian Peninsula: Evidence for subducted lithosphere below southern Spain. *Tectonophysics*, *221*, 13–34. https://doi.org/10.1016/0040-1951(93)90025-F

Bodin, T., Salmon, M., Kennett, B. L. N., & Sambridge, M. (2012). Probabilistic surface reconstruction from multiple data sets: An example for the Australian Moho. *Journal of Geophysical Research, Solid Earth*, *117*(10), 1–13. https://doi.org/10.1029/2012JB009547

Boehm, J., Werl, B., & Schuh, H. (2006). Troposphere mapping functions for GPS and very long baseline interferometry from European Centre for Medium-Range Weather Forecasts operational analysis data. *Journal of Geophysical Research, Solid Earth*, *111*, 1–9. https://doi.org/10.1029/2005JB003629

Bonnin, M., Nolet, G., Villaseñor, A., Gallart, J., & Thomas, C. (2014). Multiple-frequency tomography of the upper mantle beneath the African/Iberian collision zone. *Geophysical Journal International*, *198*(3), 1458–1473. https://doi.org/10.1093/gji/ggu214

Bosch, D., Maury, R. C., El Azzouzi, M., Bollinger, C., Bellon, H., & Verdoux, P. (2014). Lithospheric origin for Neogene-quaternary middle atlas lavas (Morocco): Clues from trace elements and Sr-Nd-Pb-Hf isotopes. *Lithos*, *205*, 247–265. https://doi.org/10.1016/j.lithos.2014.07.009

Boschi, L., Faccenna, C., & Becker, T. W. (2010). Mantle structure and dynamic topography in the Mediterranean Basin. *Geophysical Research Letters*, *37*(20), 1–6. https://doi.org/10.1029/2010GL045001

Bousquet, J. (1978). Quaternary strike-slip faults in Southeastern Spain. *Tectonophysics*, *52*, 277–286. https://doi.org/10.1016/0040-1951(79)90232-4

Braga, J. C., Martı, M., & Quesada, C. (2003). Patterns and average rates of late Neogene—Recent uplift of the. *Geomorphology*, *50*(50), 3–26. https://doi.org/10.1016/s0169-555x(02)00205-2

Bruyninx, C., Habrich, H., Söhne, W., Kenyeres A., Stangl, G., & Völksen, C. (2012). Enhancement of the EUREF Permanent Network Services and Products. In *Geodesy for Planet Earth*, *IAG Symposia Series* (Vol. 136, pp. 27–35). https://doi.org/10.1007/978-3-642-20338-1_4

Buforn, E., Coca, P., Ud, A., & Lasa, C. (1997). Source mechanism of intermediate and deep earthquakes in southern Spain. *Journal of Seismology*, 113–130. https://doi.org/10.1023/a:1009754219459

Buforn, E., de Galdeano, C. S., & Udlas, A. (1995). Seismotectonics of the Ibero-Maghrebian region. *Tectonophysics*, *248*, 247–261. https://doi.org/10.1016/0040-1951(94)00276-f

Buforn, E., Pro, C., Cesca, S., Udías, A., & Fresno, C. (2011). The 2010 Granada, Spain, deep earthquake. *Bulletin of the Seismological Society of America*, *101*(5), 2418–2430. https://doi.org/10.1785/0120110022

Buforn, E., Udias, A., Mezcua, J., & Madariaga, R. (1991). A deep earthquake under South Spain, 8 March 1990. *Bulletin de La Société Géologique de France*, *81*(4), 1403–1407.

Buontempo, L., Bokelmann, G. H. R., Barruol, G., & Morales, J. (2008). Seismic anisotropy beneath southern Iberia from *SKS* splitting. *Earth and Planetary Science Letters*, *273*(3–4), 237–250. https://doi.org/10.1016/j.epsl.2008.06.024

Calvert, A., Sandvol, E., Seber, D., Barazangi, M., Roecker, S., Mourabit, T., et al. (2000). Geodynamic evolution of the lithosphere and upper mantle beneath the Alboran region of the western Mediterranean: Constraints from travel time tomography. *Journal of Geophysical Research, Solid Earth*, *105*, 10,871–10,898. https://doi.org/10.1029/2000jb900024

Capella, W., Matenco, L., Dmitrieva, E., Roest, W. M. J., Hessels, S., Hssain, M., et al. (2017). Thick-skinned tectonics closing the Rifian corridor. *Tectonophysics*, *710–711*, 249–265. https://doi.org/10.1016/j.tecto.2016.09.028

Carballo, A., Fernandez, M., Jiménez-Munt, I., Torne, M., Vergés, J., Melchiorre, M., et al. (2015). From the north-Iberian margin to the Alboran Basin: A lithosphere geo-transect across the Iberian plate. *Tectonophysics*, *663*, 399–418. https://doi.org/10.1016/j.tecto.2015.07.009

Carlson, R. L., & Johnson, H. P. (1994). On modeling the thermal evolution of the oceanic upper mantle: An assessment of the cooling plate model. *Journal of Geophysical Research*, *99*(B2), 3201–3214. https://doi.org/10.1029/93JB02696

Casciello, E., Fernàndez, M., Vergés, J., Cesarano, M., & Torne, M. (2015). The Alboran domain in the western Mediterranean evolution: The birth of a concept. *Bulletin de la Societe Geologique de France*, *186*(4–5), 371–384. https://doi.org/10.2113/gssgfbull.186.4-5.371

Chertova, M. V., Spakman, W., Geenen, T., van den Berg, A. P., & van Hinsbergen, D. J. J. (2014). Underpinning tectonic reconstructions of the western Mediterranean region with dynamic slab evolution from 3-D numerical modeling. *Journal of Geophysical Research, Solid Earth*, *120*, 1195–1209. https://doi.org/10.1002/2014JB011376

Chevrot, S., Villasenor, A., Sylvander, M., Benahmed, S., Beucler, E., Cougoulat, G., et al. (2014). High-resolution imaging of the Pyrenees and massif central from the data of the PYROPE and IBERARRAY portable array deployments. *Journal of Geophysical Research, Solid Earth*, *119*(8), 6399–6420. https://doi.org/10.1002/2014JB010953

Civiero, C., Custódio, S., Rawlinson, N., Strak, V., Silveira, G., Arroucau, P., & Corela, C. (2019). Thermal nature of mantle upwellings below the Ibero-Western Maghreb region inferred from teleseismic tomography. *Journal of Geophysical Research, Solid Earth*, *124*(2), 1781–1801. https://doi.org/10.1029/2018JB016531

Civiero, C., Strak, V., Custódio, S., Silveira, G., Rawlinson, N., Arroucau, P., & Corela, C. (2018). A common deep source for upper-mantle upwellings below the Ibero-western Maghreb region from teleseismic P -wave travel-time tomography. *Earth and Planetary Science Letters*, *499*, 157–172. https://doi.org/10.1016/j.epsl.2018.07.024

Cunha, T. A., Matias, L. M., Terrinha, P., Negredo, A. M., Rosas, F., Fernandes, R. M. S., & Pinheiro, L. M. (2012). Neotectonics of the SW Iberia margin, gulf of Cadiz and Alboran Sea: A reassessment including recent structural, seismic and geodetic data. *Geophysical Journal International*, *188*(3), 850–872. https://doi.org/10.1111/j.1365-246X.2011.05328.x

Custódio, S., Lima, V., Vales, D., Cesca, S., & Carrilho, F. (2016). Imaging active faulting in a region of distributed deformation from the joint clustering of focal mechanisms and hypocentres: Application to the Azores – Western Mediterranean region. *Tectonophysics*, *676*, 70–89. https://doi.org/10.1016/j.tecto.2016.03.013

De Larouzière, F. D. D. E., Bolze, J. I., Bordet, P., Hernandez, J., Estevou, P. O. T. T., & Montenat, C. (1988). The Betic segment of the lithospheric trans-Alboran shear zone during the Late Miocene. *Tectonophysics*, *152*, 41–52. https://doi.org/10.1016/0040-1951(88)90028-5

de Mancilla, F. d. L., Heit, B., Morales, J., Yuan, X., Stich, D., Molina-Aguilera, A., et al. (2018). A STEP fault in central Betics, associated with lateral lithospheric tearing at the northern edge of the Gibraltar arc subduction system. *Earth and Planetary Science Letters*, *486*, 32–40. https://doi.org/10.1016/j.epsl.2018.01.008

de Mancilla, F. d. L., Stich, D., Morales, J., Martín, R., Diaz, J., Pazos, A., et al. (2015). Crustal thickness and images of the lithospheric discontinuities in the Gibraltar arc and surrounding areas. *Geophysical Journal International*, *203*(3), 1804–1820. https://doi.org/10.1093/gji/ggv390

Díaz, J., Gallart, J., & Carbonell, R. (2016). Moho topography beneath the Iberian-Western Mediterranean region mapped from controlled-source and natural seismicity surveys. *Tectonophysics*, *692*, 74–85. https://doi.org/10.1016/j.tecto.2016.08.023

Díaz, J., & Gallart, J. (2009). Crustal structure beneath the Iberian Peninsula and surrounding waters: A new compilation of deep seismic sounding results. *Physics of the Earth and Planetary Interiors*, *173*(1–2), 181–190. https://doi.org/10.1016/j.pepi.2008.11.008

Díaz, J., & Gallart, J. (2014). Seismic anisotropy from the Variscan core of Iberia to the Western African Craton: New constrains on upper mantle flow at regional scales. *Earth and Planetary Science Letters*, *394*, 48–57. https://doi.org/10.1016/j.epsl.2014.03.005

Díaz, J., Gallart, J., Morais, I., Silveira, G., Pedreira, D., Pulgar, J. A., et al. (2015). From the Bay of Biscay to the high atlas: Completing the anisotropic characterization of the upper mantle beneath the westernmost Mediterranean region. *Tectonophysics*, *663*, 192–202. https://doi.org/10.1016/j.tecto.2015.03.007

Díaz, J., Gallart, J., Villaseñor, A., Mancilla, F., Pazos, A., Córdoba, D., et al. (2010). Mantle dynamics beneath the Gibraltar are (western Mediterranean) from shear-wave splitting measurements on a dense seismic array. *Geophysical Research Letters*, *37*(18), 1–5. https://doi.org/10.1029/2010GL044201

Díaz, J., Gil, A., Carbonell, R., Gallart, J., & Harnafi, M. (2016). Constraining the crustal root geometry beneath northern Morocco. *Tectonophysics*, *689*, 14–24. https://doi.org/10.1016/j.tecto.2015.12.009

Duarte, J. C., Rosas, F. M., Terrinha, P., Schellart, W. P., Boutelier, D., Gutscher, M. A., & Ribeiro, A. (2013). Are subduction zones invading the Atlantic? Evidence from the Southwest Iberia margin. *Geology*, *41*(8), 839–842. https://doi.org/10.1130/G34100.1

Duggen, S., Hoernle, K., van den Bogaard, P., & Garbe-Schönberg, D. (2005). Post-collisional transition from subduction-to intraplate-type magmatism in the westernmost Mediterranean: Evidence for continental-edge delamination of subcontinental lithosphere. *Journal of Petrology*, *46*(6), 1155–1201. https://doi.org/10.1093/petrology/egi013

Duggen, S., Hoernle, K., van den Bogaard, P., & Harris, C. (2004). Magmatic evolution of the Alboran region: The role of subduction in forming the western Mediterranean and causing the Messinian salinity crisis. *Earth and Planetary Science Letters*, *218*(1–2), 91–108. https://doi.org/10.1016/S0012-821X(03)00632-0

Duggen, S., Hoernle, K., van den Bogaard, P., Ruuüpke, L., & Morgan, J. P. (2003). Deep roots of the Messinian salinity crisis. *Nature*, *422*(6932). https://doi.org/10.1038/nature01551.1

Dündar, S., Dias, N. A., Silveira, G., Kind, R., Vinnik, L., Matias, L., & Bianchi, M. (2016). Estimation of the crustal bulk properties beneath mainland Portugal from *P*-wave Teleseismic receiver functions. *Pure and Applied Geophysics*, *173*(6), 1949–1970. https://doi.org/10.1007/s00024-016-1257-4

El Moudnib, L., Villaseñor, A., Harnafi, M., Gallart, J., Pazos, A., Serrano, I., et al. (2015). Crustal structure of the Betic-Rif system, western Mediterranean, from local earthquake tomography. *Tectonophysics*, *643*, 94–105. https://doi.org/10.1016/j.tecto.2014.12.015

Faccenna, C., & Becker, T. W. (2010). Shaping mobile belts by small-scale convection. *Nature*, *465*(7298), 602–605. https://doi.org/10.1038/nature09064

Faccenna, C., Becker, T. W., Auer, L., Billi, A., Boschi, L., Brun, J. P., et al. (2014). Mantle dynamics in the Mediterranean. *Reviews of Geophysics*, *52*(3), 283–332. https://doi.org/10.1002/2013rg000444

Faccenna, C., Molin, P., Orecchio, B., Olivetti, V., Bellier, O., Funiciello, F., et al. (2011). Topography of the Calabria subduction zone (southern Italy): Clues for the origin of Mt. Etna. *Tectonics*, *30*(1), 1–20. https://doi.org/10.1029/2010TC002694

Faccenna, C., Piromallo, C., Crespo-blanc, A., & Jolivet, L. (2004). Lateral slab deformation and the origin of the western Mediterranean arcs. *Tectonics*, *23*. https://doi.org/10.1029/2002TC001488

Fadil, A., Vernant, P., Mcclusky, S., Reilinger, R., Gomez, F., Ben Sari, D., et al. (2006). Active tectonics of the western Mediterranean: Geodetic evidence for rollback of a delaminated subcontinental lithospheric slab beneath the Rif Mountains, Morocco. *Geology*, *7*, 529–532. https://doi.org/10.1130/G22291.1

Fernandes, R. M. S., Ambrosius, B. A. C., Noomen, R., Bastos, L., Wortel, M. J. R., Spakman, W., & Govers, R. (2003). The relative motion between Africa and Eurasia as derived from ITRF2000 and GPS data. *Geophysical Research Letters*, *30*(16), 1–5. https://doi.org/10.1029/2003GL017089

Fernandez, J., Prieto, J. F., Escayo, J., Camacho, A. G., Luzón, F., Tiampo, K. F., et al. (2018). Modeling the two- and three- dimensional displacement field in Lorca, Spain, subsidence and the global implications. *Scientific Reports, (June)*, *8*(1). https://doi.org/10.1038/s41598-018-33128-0

Fullea, J., Fernàndez, M., Afonso, J. C., Vergés, J., & Zeyen, H. (2010). The structure and evolution of the lithosphere-asthenosphere boundary beneath the Atlantic-Mediterranean transition region. *Lithos*, *120*(1–2), 74–95. https://doi.org/10.1016/j.lithos.2010.03.003

Funiciello, F., Moroni, M., Piromallo, C., Faccenna, C., Cenedese, A., & Bui, H. A. (2006). Mapping mantle flow during retreating subduction: Laboratory models analyzed by feature tracking. *Journal of Geophysical Research, Solid Earth*, *111*(3), 1–16. https://doi.org/10.1029/2005JB003792

Garate, J., Martin-Davila, J., Khazaradze, G., Echeverria, A., Asensio, E., Gil, A. J., et al. (2015). Topo-Iberia project: CGPS crustal velocity field in the Iberian Peninsula and Morocco. *GPS Solutions*, *19*(2), 287–295. https://doi.org/10.1007/s10291-014-0387-3

Garcia-Castellanos, D., & Villaseñor, A. (2011). Messinian salinity crisis regulated by competing tectonics and erosion at the Gibraltar arc. *Nature*, *480*(7377), 359–363. https://doi.org/10.1038/nature10651

Gill, R. C. O., Aparicio, A., El Azzouzi, M., Hernandez, J., Thirlwall, M. F., Bourgois, J., & Marriner, G. F. (2004). Depleted arc volcanism in the Alboran Sea and shoshonitic volcanism in Morocco: Geochemical and isotopic constraints on Neogene tectonic processes. *Lithos*, *78*(4), 363–388. https://doi.org/10.1016/j.lithos.2004.07.002

Gutscher, M.-A., Dominguez, S., Westbrook, G. K., Le Roy, P., Rosas, F., Duarte, J. C., et al. (2012). Tectonophysics the Gibraltar subduction: A decade of new geophysical data. *Tectonophysics*, *574–575*, 72–91. https://doi.org/10.1016/j.tecto.2012.08.038

Gutscher, M. A., Malod, J., Rehault, J. P., Contrucci, I., Klingelhoefer, F., Mendes-Victor, L., & Spakman, W. (2002). Evidence for active subduction beneath Gibraltar. *Geology*, *30*(12), 1071–1074. https://doi.org/10.1130/0091-7613(2002)030%3C1071:EFASBG%3E2.0.CO;2

Hager, B. H., Clayton, R. W., Richards, M. A., Comer, R. P., & Dziewonskft, A. M. (1984). Erratum: Lower mantle heterogeneity, dynamic topography and the geoid. *Nature*, *314*(6013), 752. https://doi.org/10.1038/314752a0

Herring, T. (2003). MATLAB tools for viewing GPS velocities and time series. *GPS Tool Box*, *7*(1), 194–199. https://doi.org/10.1007/s10291-003-0068-0

Herring, T. A., King, R. W., Floyd, M. A., & McClusky, S. C. (2015). *GAMIT-GPS analysis at MIT, reference manual 10.6*. Department of Earth, Atmospheric, and Planetary Sciences Massachusetts Institute of Technology. Retrieved from http://www-gpsg.mit.edu

Houseman, G. (1996). From mountains to basin. *Nature*, *379*(6568), 771–772. https://doi.org/10.1038/379771a0

Iribarren, L., Vergés, J., Camurri, F., Fullea, J., & Fernàndez, M. (2007). The structure of the Atlantic-Mediterranean transition zone from the Alboran Sea to the horseshoe abyssal plain (Iberia-Africa plate boundary). *Marine Geology*, *243*(1–4), 97–119. https://doi.org/10.1016/j.margeo.2007.05.011

Iribarren, L., Vergés, J., & Fernàndez, M. (2009). Sediment supply from the Betic-Rif orogen to basins through Neogene. *Tectonophysics*, *475*(1), 68–84. https://doi.org/10.1016/j.tecto.2008.11.029

Jiménez-Munt, I., & Negredo, A. M. (2003). Neotectonic modelling of the western part of the Africa-Eurasia plate boundary: From the mid-Atlantic ridge to Algeria. *Earth and Planetary Science Letters*, *205*(3–4), 257–271. https://doi.org/10.1016/S0012-821X(02)01045-2

Johansson, J. M. (2002). Continuous GPS measurements of postglacial adjustment in Fennoscandia 1. Geodetic results. *Journal of Geophysical Research, Solid Earth*, *107*(B8), 2157. https://doi.org/10.1029/2001JB000400

Johnston, G., Riddell, A., & Hausler, G. (2017). The international GNSS service. In P. J. G. Teunissen, & O. Montenbruck (Eds.), *Springer Handbook of Global Navigation Satellite Systems*, (pp. 967–982). Cham: Springer International Publishing.

Koulali, A., Ouazar, D., Tahayt, A., King, R. W., Vernant, P., Reilinger, R. E., et al. (2011). New GPS constraints on active deformation along the Africa-Iberia plate boundary. *Earth and Planetary Science Letters*, *308*(1–2), 211–217. https://doi.org/10.1016/j.epsl.2011.05.048

Krijgsman, W., Hilgen, F. J., Raffi, I., Sierro, F. J., & Wilson, D. S. (1999). Chronology, causes and progression of the Messinian salinity crisis. *Nature*, *400*(6745), 652–655. https://doi.org/10.1038/23231

Lagler, K., Schindelegger, M., Böhm, J., Krásná, H., & Nilsson, T. (2013). GPT2: Empirical slant delay model for radio space geodetic techniques. *Geophysical Research Letters*, *40*, 1069–1073. https://doi.org/10.1002/grl.50288

Larson, M., & van Dam, T. (2000). Measuring postglacial rebound with GPS and absolute gravity. *Geophysical Research Letters*, *27*(23), 3925–3928. https://doi.org/10.1029/2000GL011946

Laske, G., Masters, G., Ma, Z., & Pasyanos, M. E. (2013). *CRUST1.0: An updated global model of Earth's crust* (Vol. 15). Geophysical Research Abstracts, Vienna, Austria: European Geoscience Union. Abstract EGU2013-2658. Retrieved from http://igppweb.ucsd.edu/~gabi/rem.html

Leblanc, D., & Olivier, P. H. (1984). Role of strike-slip faults in the Betic-Rifian orogeny. *Tectonophysics*, *101*, 345–355. https://doi.org/10.1016/0040-1951(84)90120-3

Levander, A., Bezada, M. J., Niu, F., Humphreys, E. D., Palomeras, I., Thurner, S. M., et al. (2014). Subduction-driven recycling of continental margin lithosphere. *Nature*, *515*(7526), 253–256. https://doi.org/10.1038/nature13878

Li, Z. H., & Ribe, N. M. (2012). Dynamics of free subduction from 3-D boundary element modeling. *Journal of Geophysical Research, Solid Earth*, *117*(6), 1–18. https://doi.org/10.1029/2012JB009165

Lonergan, L., & White, N. (1997). Origin of the Betic-Rif mountain belt. *Tectonics*, *16*(3), 504–522. https://doi.org/10.1029/96TC03937

Lowry, A. R., Hamburger, M. W., Meertens, C. M., & Ramos, E. G. (2001). GPS monitoring of crustal deformation at Taal volcano, Philippines. *Journal of Volcanology and Geothermal Research*, *105*, 35–47. https://doi.org/10.1016/S0377-0273(00)00238-9

Lustrino, M., Duggen, S., & Rosenberg, C. L. (2011). The Central-Western Mediterranean: Anomalous igneous activity in an anomalous collisional tectonic setting. *Earth-Science Reviews*, *104*(1–3), 1–40. https://doi.org/10.1016/j.earscirev.2010.08.002

Lustrino, M., & Wilson, M. (2007). The circum-Mediterranean anorogenic Cenozoic igneous province. *Earth-Science Reviews*, *81*, 1–65. https://doi.org/10.1016/j.earscirev.2006.09.002

Lyard, F., Lefevre, F., & Letellier, T. (2006). Modelling the global ocean tides: Modern insights from FES2004. *Ocean Dynamics*, 394–415. https://doi.org/10.1007/s10236-006-0086-x

Malinverno, A., & Ryan, W. B. F. (1986). Extension in the Tyrrhenian Sea and shortening in the Apennines as result of arc migration driven by sinking of the lithosphere. *Tectonics*, *5*(2), 227–245. https://doi.org/10.1029/TC005i002p00227

Mancilla, F., & Diaz, J. (2015). High resolution Moho topography map beneath Iberia and northern Morocco from receiver function analysis. *Tectonophysics*, *663*, 203–211. https://doi.org/10.1016/j.tecto.2015.06.017

Mancilla, F. d. L., Stich, D., Morales, J., Julià, J., Diaz, J., Pazos, A., et al. (2012). Crustal thickness variations in northern Morocco. *Journal of Geophysical Research, Solid Earth*, *117*, 1–14. https://doi.org/10.1029/2011JB008608

Mancilla, F., Stich, D., Berrocoso, M., Martín, R., Morales, J., Fernandez-Ros, A., et al. (2013). Delamination in the Betic range: Deep structure, seismicity, and GPS motion. *Geology*, 307–310. https://doi.org/10.1130/G33733.1

Martín, R., Stich, D., Morales, J., & Mancilla, F. (2015). Moment tensor solutions for the Iberian-Maghreb region during the IberArray deployment (2009–2013). *Tectonophysics*, *663*, 261–274. https://doi.org/10.1016/j.tecto.2015.08.012

Martínez-Loriente, S., Sallarès, V., Gràcia, E., Bartolomé, R., Dañobeitia, J. J., & Zitellini, N. (2014). Seismic and gravity constraints on the nature of the basement in the Africa-Eurasia Plate boundary: New insights for the geodynamic evolution of the SW Iberian margin. *Journal of Geophysical Research, Solid Earth*, *119*(1), 127–149. https://doi.org/10.1002/2013jb010476

Mattei, M., Cifelli, F., Rojas, I. M., Crespo Blanc, A., Comas, M., Faccenna, C., & Porreca, M. (2006). Neogene tectonic evolution of the Gibraltar arc: New paleomagnetic constrains from the Betic chain. *Earth and Planetary Science Letters*, *250*(3–4), 522–540. https://doi.org/10.1016/j.epsl.2006.08.012

Maury, R., Fourcade, S., Coulon, C., El Azzouzi, M., Bellon, H., Coutelle, A., et al. (2000). Post-collisional Neogene magmatism of the Mediterranean Maghreb margin: A consequence of slab breakoff. *Comptes Rendus de l'Academie de Sciences - Serie IIa: Sciences de La Terre et Des Planetes*, *331*(3), 159–173. https://doi.org/10.1016/S1251-8050(00)01406-3

Megies, T., Beyreuther, M., Barsch, R., Krischer, L., & Wassermann, J. (2011). ObsPy—What can it do for data centers and observatories? *Annals of Geophysics*, *54*(1), 47–58. https://doi.org/10.4401/ag-4838

Miller, M. S., Allam, A. A., Becker, T. W., Di Leo, J. F., & Wookey, J. (2013). Constraints on the tectonic evolution of the westernmost Mediterranean and northwestern Africa from shear wave splitting analysis. *Earth and Planetary Science Letters*, *375*, 234–243. https://doi.org/10.1016/j.epsl.2013.05.036

Molina-Aguilera, A., de Lis Mancilla, F., Morales, J., Stich, D., Yuan, X., & Heit, B. (2019). Connection between the Jurassic oceanic lithosphere of the Gulf of Cádiz and the Alboran slab imaged by Sp receiver functions. *Geology*, *47*(3), 227–230. https://doi.org/10.1130/g45654.1

Molinari, I., & Morelli, A. (2011). EPcrust: A reference crustal model for the European plate. *Geophysical Journal International*, *185*(1), 352–364. https://doi.org/10.1111/j.1365-246X.2011.04940.x

Molnar, P., & England, P. (1990). Late Cenozoic uplift of mountain ranges and global climate change: Chicken or egg? *Nature*, *346*. https://doi.org/10.1038/346029a0

Monna, S., Cimini, G. B., Montuori, C., Matias, L., Geissler, W. H., & Favali, P. (2013). New insights from seismic tomography on the complex geodynamic evolution of two adjacent domains: Gulf of Cadiz and Alboran Sea. *Journal of Geophysical Research, Solid Earth*, *118*(4), 1587–1601. https://doi.org/10.1029/2012JB009607

Neres, M., Carafa, M. M. C., Fernandes, R. M. S., Matias, L., Duarte, J. C., Barba, S., & Terrinha, P. (2016). Lithospheric deformation in the Africa-Iberia plate boundary: Improved neotectonic modeling testing a basal-driven Alboran plate. *Journal of Geophysical Research, Solid Earth*, *121*(9), 6566–6596. https://doi.org/10.1002/2016JB013012

Nocquet, J. M., Calais, E., & Parsons, B. (2005). Geodetic constraints on glacial isostatic adjustment in Europe. *Geophysical Research Letters*, *32*(6), 1–5. https://doi.org/10.1029/2004GL022174

Palano, M., González, P. J., & Fernández, J. (2013). Strain and stress fields along the Gibraltar Orogenic arc: Constraints on active geodynamics. *Gondwana Research*, *23*(3), 1071–1088. https://doi.org/10.1016/j.gr.2012.05.021

Palomeras, I., Thurner, S., Levander, A., Liu, K., Villasenor, A., Carbonell, R., & Harnafi, M. (2014). Finite-frequency Rayleigh wave tomography of the western Mediterranean: Mapping its lithospheric structure. *Geochemistry, Geophysics, Geosystems*, *15*(1), 140–160. https://doi.org/10.1002/2013GC004861

Palomeras, I., Villaseñor, A., Thurner, S., Levander, A., Gallart, J., & Harnafi, M. (2017). Lithospheric structure of Iberia and Morocco using finite-frequency Rayleigh wave tomography from earthquakes and seismic ambient noise. *Geochemistry, Geophysics, Geosystems*, *18*(5), 1824–1840. https://doi.org/10.1002/2016GC006657

Peltier, W. R., Argus, D. F., & Drummond, R. (2015). Theoretical modeling insights into elastic wave attenuation mechanisms in marine sediments with pore-filling methane hydrate. *Journal of Geophysical Research, Solid Earth*, *2015*(120), 450–487. https://doi.org/10.1002/2016jb013577

Pérouse, E., Vernant, P., Chéry, J., Reilinger, R., & McClusky, S. (2010). Active surface deformation and sub-lithospheric processes in the western Mediterranean constrained by numerical models. *Geology*, *38*(9), 823–826. https://doi.org/10.1130/G30963.1

Petit, C., Le Pourhiet, L., Scalabrino, B., Corsini, M., Bonnin, M., & Romagny, A. (2015). Crustal structure and gravity anomalies beneath the Rif, northern Morocco: Implications for the current tectonics of the Alboran region. *Geophysical Journal International*, *202*(1), 640–652. https://doi.org/10.1093/gji/ggv169

Piromallo, C., Becker, T. W., Funiciello, F., & Faccenna, C. (2006). Three-dimensional instantaneous mantle flow induced by subduction. *Geophysical Research Letters*, *33*(8), 5–8. https://doi.org/10.1029/2005GL025390

Piromallo, C., & Morelli, A. (2003). *P* wave tomography of the mantle under the Alpine-Mediterranean area. *Journal of Geophysical Research, Solid Earth*, *108*(B2), 1–23. https://doi.org/10.1029/2002JB001757

Platt, J. P., Behr, W. M., Johanesen, K., & Williams, J. R. (2013). The Betic-Rif arc and its Orogenic hinterland: A review. *Annual Review of Earth and Planetary Sciences*, *41*, 313–357. https://doi.org/10.1146/annurev-earth-050212-123951

Platt, J. P., Soto, J., Whitehouse, M. J., Hurford, A. J., Kelley, S. P., & Conrad, D. (1998). Thermal evolution, rate of exhumation, and tectonic significance of metamorphic rocks from the floor of the Alboran extensional basin, western Mediterranean. *Tectonics*, *17*(5), 671–689. https://doi.org/10.1029/98TC02204

Platt, J. P., & Vissers, R. L. M. (1989). Extensional collapse of thickened continental lithosphere: A working hypothesis for the Alboran Sea and Gibraltar arc. *Geology*, *17*(6), 540–543. https://doi.org/10.1130/0091-7613(1989)017%3C0540:ecotcl%3E2.3.co;2

Pulido-Bosch, A., Delgado, J., Sola, F., Vallejos, Á., Vicente, F., López-Sánchez, J. M., & Mallorquí, J. J. (2012). Identification of potential subsidence related to pumping in the Almería basin (SE Spain). *Hydrological Processes*, *26*(5), 731–740. https://doi.org/10.1002/hyp.8181

Rehault, J.-P., Boillot, G., & Mauffret, A. (1985). The Western Mediterranean Basin. In *Geological evolution of the Mediterranean Basin*, (pp. 101–129). New York, NY: Springer New York.

Rosenbaum, G., Lister, G. S., & Duboz, C. (2002). Relative motions of Africa, Iberia and Europe during Alpine orogeny. *Tectonophysics*, *359*, 117–129. https://doi.org/10.1016/S0040-1951(02)00442-0

Royden, L. H. (1993). The tectonic expression slab pull at continental convergent boundaries. *Tectonics*, *12*(3), 629–638. https://doi.org/10.1029/92tc02248

Salah, M. K. (2014). Upper crustal structure beneath Southwest Iberia north of the convergent boundary between the Eurasian and African plates. *Geoscience Frontiers*, *5*(6), 845–854. https://doi.org/10.1016/j.gsf.2013.10.002

Sallarès, V., Gailler, A., Gutscher, M.-A., Graindorge, D., Bartolomé, R., Gràcia, E., et al. (2011). Seismic evidence for the presence of Jurassic oceanic crust in the central gulf of Cadiz (SW Iberian margin). *Earth and Planetary Science Letters*, *311*(1–2), 112–123. https://doi.org/10.1016/j.epsl.2011.09.003

Santos-Bueno, N., Fernández-García, C., Stich, D., de Lis Mancilla, F., Martín, R., Molina-Aguilera, A., & Morales, J. (2019). Focal mechanisms for subcrustal earthquakes beneath the Gibraltar arc. *Geophysical Research Letters*, *46*(5), 2534–2543. https://doi.org/10.1029/2018GL081587

Sanz de Galdeano, C. (1990). Geologic evolution of the Betic cordilleras in the Western Mediterranean, Miocene to the present. *Tectonophysics*, *172*, 107–119. https://doi.org/10.1016/0040-1951(90)90062-D

Sanz de Galdeano, C., & Alfaro, P. (2004). Tectonic significance of the present relief of the Betic cordillera. *Geomorphology*, *63*(3–4), 175–190. https://doi.org/10.1016/j.geomorph.2004.04.002

Schellart, W. P. (2008). Kinematics and flow patterns in deep mantle and upper mantle subduction models: Influence of the mantle depth and slab to mantle viscosity ratio. *Geochemistry, Geophysics, Geosystems*, *9*(3), Q03014. https://doi.org/10.1029/2007GC001656

Schellart, W. P., & Lister, G. S. (2004). Tectonic models for the formation of arc-shaped convergent zones and backarc basins. In A. J. Sussman & A. B. Weil (Eds.), *Orogenic Curvature: Integrating Paleomagnetic and Structural Analyses* (Vol. 383, pp. 237–258). Geol. Soc. Am. Spec. Pap.

Scherneck, H., Johansson, J. M., Vermeer, M., Davis, J. L., Milne, G. A., & Mitrovica, J. X. (2001). BIFROST project: 3-D crustal deformation rates derived from GPS confirm postglacial rebound in Fennoscandia. *Earth, Planets and Space*, *53*(7), 703–708. https://doi.org/10.1186/BF03352398

Seber, D., Barazangi, M., Tadili, B. A., Ramdani, M., Ibenbrahim, A., Sari, D. B., & Ben Sari, D. (1996). Three-dimensional upper mantle structure beneath the intraplate atlas and interplate Rif mountains of Morocco. *Journal of Geophysical Research*, *101*(B2), 3125. https://doi.org/10.1029/95JB03112

Serpelloni, E., Faccenna, C., Spada, G., Dong, D., & Williams, S. D. P. (2013). Vertical GPS ground motion rates in the Euro-Mediterranean region: New evidence of velocity gradients at different spatial scales along the Nubia-Eurasia plate boundary. *Journal of Geophysical Research, Solid Earth*, *118*, 6003–6024. https://doi.org/10.1002/2013JB010102

Simmons, N. A., Myers, S. C., Johannesson, G., & Matzel, E. (2012). LLNL-G3Dv3: Global P wave tomography model for improved regional and teleseismic travel time prediction. *Journal of Geophysical Research, Solid Earth*, *117*(10). https://doi.org/10.1029/2012JB009525

Smith, W. H., & Sandwell, D. (1997). Global Sea floor topography from satellite altimetry and ship depth soundings. *Science*, *277*(5334), 1956–1962. https://doi.org/10.1126/science.277.5334.1956

Spakman, W., Chertova, M. V., van den Berg, A., & van Hinsbergen, D. J. J. (2018). Puzzling features of western Mediterranean tectonics explained by slab dragging. *Nature Geoscience*, *11*(3), 211–216. https://doi.org/10.1038/s41561-018-0066-z

Spakman, W., & Wortel, R. (2004). A tomographic view on Western Mediterranean geodynamics. In *The TRANSMED Atlas. The Mediterranean region from crust to mantle* (pp. 31–52). Berlin - Heidelberg, Germany: Springer-Verlag.

Stegman, D. R., Freeman, J., Schellart, W. P., Moresi, L., & May, D. (2006). Influence of trench width on subduction hinge retreat rates in 3-D models of slab rollback. *Geochemistry, Geophysics, Geosystems*, *7*(3), Q03012. https://doi.org/10.1029/2005GC001056

Stich, D., Mancilla, F. D. L., & Morales, J. (2005). Crust-mantle coupling in the Gulf of Cadiz (SW-Iberia). *Geophysical Research Letters*, *32*, 2–5. https://doi.org/10.1029/2005GL023098

Stich, D., Martínez-Solares, J. M., Custódio, S., Batlló, J., Martín, R., Teves-Costa, P., & Morales, J. (2020). Seismicity of the Iberian Peninsula. In *The geology of Iberia: A geodynamic approach*, (pp. 11–32). Cham: Springer.

Stich, D., Serpelloni, E., De Lis, F., & Morales, J. (2006). Kinematics of the Iberia—Maghreb plate contact from seismic moment tensors and GPS observations. *Tectonophysics*, *426*, 295–317. https://doi.org/10.1016/j.tecto.2006.08.004

Strak, V., & Schellart, W. P. (2014). Evolution of 3-D subduction-induced mantle flow around lateral slab edges in analogue models of free subduction analysed by stereoscopic particle image velocimetry technique. *Earth and Planetary Science Letters*, *403*, 368–379. https://doi.org/10.1016/j.epsl.2014.07.007

Tahayt, A., Mourabit, T., Rigo, A., Feigl, K. L., Fadil, A., Mcclusky, S., et al. (2008). Mouvements actuels des blocs tectoniques dans l' arc Bético-Rifain à partir des mesures GPS entre 1999 et 2005. *Comptes Rendus de l'Academie de Sciences - Serie IIa: Sciences de La Terre et Des Planetes*, *340*, 400–413. https://doi.org/10.1016/j.crte.2008.02.003

Tape, C., Musé, P., Simons, M., Dong, D., & Webb, F. (2009). Multiscale estimation of GPS velocity fields. *Geophysical Journal International*, *179*(2), 945–971. https://doi.org/10.1111/j.1365-246X.2009.04337.x

Teferle, F. N., Bingley, R. M., Williams, S. D. P., Baker, T. F., & Dodson, A. H. (2006). Using continuous GPS and absolute gravity to separate vertical land movements and changes in sea-level at tide-gauges in the UK. *Philosophical Transactions of the Royal Society A: Mathematical, Physical and Engineering Sciences (February)*, *364*(1841), 917–930. https://doi.org/10.1098/rsta.2006.1746

Thiebot, E., & Gutscher, M. A. (2006). The Gibraltar arc seismogenic zone (Part 1): Constraints on a shallow east dipping fault plane source for the 1755 Lisbon earthquake provided by seismic data, gravity and thermal modeling. *Tectonophysics*, *426*(1–2, 152), 135. https://doi.org/10.1016/j.tecto.2006.02.024

Thurner, S., Palomeras, I., Levander, A., Carbonell, R., & Lee, C. T. (2014). Ongoing lithospheric removal in the western Mediterranean: Evidence from Ps receiver functions and thermobarometry of Neogene basalts (PICASSO project). *Geochemistry, Geophysics, Geosystems*, *15*(4), 1113–1127. https://doi.org/10.1002/2013GC005124

Van Hinsbergen, D. J. J., Vissers, R. L. M., & Spakman, W. (2014). Origin and consequences of western Mediterranean subduction, rollback, and slab segmentation. *Tectonics*, *33*(4), 393–419. https://doi.org/10.1002/2013TC003349

Vergés, J., & Fernàndez, M. (2012). Tectonophysics tethys—Atlantic interaction along the Iberia–Africa plate boundary: The Betic–Rif orogenic system. *Tectonophysics*, *579*, 144–172. https://doi.org/10.1016/j.tecto.2012.08.032

Vernant, P., Fadil, A., Mourabit, T., Ouazar, D., Koulali, A., Davila, J. M., et al. (2010). Geodetic constraints on active tectonics of the Western Mediterranean: Implications for the kinematics and dynamics of the Nubia-Eurasia plate boundary zone. *Journal of Geodynamics*, *49*(3–4), 123–129. https://doi.org/10.1016/j.jog.2009.10.007

Vilanova, S. P., Nemser, E. S., Besana-Ostman, G. M., Bezzeghoud, M., Borges, J. F., da Silveira, A. B., et al. (2014). Incorporating descriptive metadata into seismic source zone models for seismic-hazard assessment: A case study of the Azores-west Iberian region. *Bulletin of the Seismological Society of America*, *104*(3), 1212–1229. https://doi.org/10.1785/0120130210

Wessel, P., & Smith, H. F. (1995). New version of the generic mapping tools released. *Eos, Transactions American Geophysical Union*, *76*(33), 329–336. https://doi.org/10.1029/95EO00198

Williams, J. R., & Platt, J. P. (2018). A new structural and kinematic framework for the Alborán domain (Betic–Rif arc, western Mediterranean orogenic system). *Journal of the Geological Society*, *175*(3), 465–496. https://doi.org/10.1144/jgs2017-086

Wöppelmann, G., Miguez, B. M., Bouin, M., & Altamimi, Z. (2007). Geocentric Sea-level trend estimates from GPS analyses at relevant tide gauges world-wide. *Global and Planetary Change*, *57*, 396–406. https://doi.org/10.1016/j.gloplacha.2007.02.002

Wortel, M. J. R., & Spakman, W. (2000). Subduction and slab detachment in the Mediterranean-Carpathian region. *Science*, *290*(5498), 1910–1917. https://doi.org/10.1126/science.290.5498.1910

Zeck, H. P. (1996). Betic-Rif orogeny: Subduction of Mesozoic Tethys lithosphere under eastward drifting Iberia, slab detachment shortly before 22 Ma, and subsequent uplift and extensional tectonics. *Tectonophysics*, *254*(1–2), 1–16. https://doi.org/10.1016/0040-1951(95)00206-5

Zitellini, N., Gràcia, E., Matias, L., Terrinha, P., Abreu, M. A., De Alteriis, G., et al. (2009). The quest for the Africa-Eurasia plate boundary west of the strait of Gibraltar. *Earth and Planetary Science Letters*, *280*(1–4), 13–50. https://doi.org/10.1016/j.epsl.2008.12.005